12

B S

SYSTEMS, SCIENCE AND SOFTWARE

SSS-R-77-3345

SEISMIC STUDIES FOR IMPROVED YIELD DETERMINATION

T. C. Bache
P. L. Goupillaud
B. F. Mason

Quarterly Technical Report
For Period April 1 - June 30, 1977

Sponsored by
Advanced Research Projects Agency
ARPA Order No. 2551

This research was supported by the Advanced Research Projects Agency of the Department of Defense and was monitored by AFTAC/VSC, Patrick Air Force Base, Flordia, 32925, under Contract No. F08606-76-C-0041.

July 1977

P. O. BOX 1620, LA JOLLA, CALIFORNIA 92038, TELEPHONE (714) 453-0060

AFTAC Project Authorization No. VELA/T/7712/B/ETR

Program Code No. 6H189

Effective Date of Contract: October 1, 1976

Contract Expiration Date: September 30, 1977

Amount of Contract: $410,412

Contract No. F08606-76-C-0041

Principal Investigator and Phone No.
Dr. Thomas C. Bache, (714) 453-0060, Ext. 337

Project Scientist and Phone No.
Dr. Ralph W. Alewine, III, (202) 325-8484

UNCLASSIFIED

SECURITY CLASSIFICATION OF THIS PAGE (When Data Entered)

REPORT DOCUMENTATION PAGE

READ INSTRUCTIONS BEFORE COMPLETING FORM

1. REPORT NUMBER

2. GOVT ACCESSION NO.

3. RECIPIENT'S CATALOG NUMBER

4. TITLE (and Subtitle)

(6) SEISMIC STUDIES FOR IMPROVED YIELD DETERMINATION.

5. TYPE OF REPORT & PERIOD COVERED

Quarterly Report
April 1-June 30, 1977

6. PERFORMING ORG. REPORT NUMBER

(14) SSS-R-77-3345

7. AUTHOR(s)

(Thomas) (10) T. C. Bache,
P. L. Goupillaud
B. F. Mason

8. CONTRACT OR GRANT NUMBER(s)

(15) F08606-76-C-0041
ARPA Order-2551

9. PERFORMING ORGANIZATION NAME AND ADDRESS

Systems, Science and Software
P. O. Box 1620
La Jolla, California 92038

10. PROGRAM ELEMENT, PROJECT, TASK AREA & WORK UNIT NUMBERS

Program Code 6H189
Project Authorization
No. VELA/T/7712/B/ETR

11. CONTROLLING OFFICE NAME AND ADDRESS

VELA Seismological Center
312 Montgomery Street
Alexandria, Virginia 22314

(11) 12. REPORT DATE

July 1977

13. NUMBER OF PAGES

65

(9) 14. MONITORING AGENCY NAME & ADDRESS (if different from Controlling Office)

Quarterly technical rept.
1 Apr - 30 Jun 77

15. SECURITY CLASS. (of this report)

Unclassified

15a. DECLASSIFICATION/DOWNGRADING SCHEDULE

16. DISTRIBUTION STATEMENT (of this Report)

(12) 73p.

Approved for Public Release, Distribution Unlimited

17. DISTRIBUTION STATEMENT (of the abstract entered in Block 20, if different from Report)

18. SUPPLEMENTARY NOTES

19. KEY WORDS (Continue on reverse side if necessary and identify by block number)

Seismic surface waves
M_S versus yield
Theoretical seismogram generation
Seismic signal deconvolution

20. ABSTRACT (Continue on reverse side if necessary and identify by block number)

Results are presented from research conducted during the quarter from April to June 1977. Work in three research areas is discussed in the following areas:

(1) The dependence of observed surface wave amplitudes on explosion yield and the characteristics of the emplacement medium is reviewed. Surface wave data compiled by others is used in

(cont on p 1473B)

DD FORM 1 JAN 73 1473 EDITION OF 1 NOV 65 IS OBSOLETE

UNCLASSIFIED

SECURITY CLASSIFICATION OF THIS PAGE (When Data Entered)

388 507

6B

(cont'd from p 1473A)

20. ABSTRACT (cont'd)

conjunction with a new data set consisting of Airy phase amplitudes from the WWSSN stations ALQ and TUC;

(2) The theoretical dependence of surface wave amplitude on the important controlling parameters is discussed. Attention is directed to the assumptions of the theoretical models and their consequences; and

(3) Preliminary results are presented for the development and testing of a deconvolution technique for analyzing short period teleseismic recordings of explosions.

(1473B)

ABSTRACT

Results are presented from research conducted during the quarter from April to June 1977. Work in three research areas is discussed:

1. The dependence of observed surface wave amplitudes on explosion yield and the characteristics of the emplacement medium is reviewed. Surface wave data compiled by others is used in conjunction with a new data set consisting of Airy phase amplitudes from the WWSSN stations ALQ and TUC.

2. The theoretical dependence of surface wave amplitude on the important controlling parameters is discussed. Attention is directed to the assumptions of the theoretical models and their consequences.

3. Preliminary results are presented for the development and testing of a deconvolution technique for analyzing short period teleseismic recordings of explosions.

TABLE OF CONTENTS

LIST OF ILLUSTRATIONS

LIST OF ILLUSTRATIONS (continued)

I. SUMMARY

The objective of our research program is to examine the parameters that affect the seismic signals from underground explosions. Our attention is primarily directed to those features of the seismic waveforms that reliably indicate the explosion yield. Our research program includes empirical studies of the available data, experimental studies using small charges to simulate explosions and the development and application of theoretical and numerical methods. Emphasis is on the latter. In particular, we are applying techniques for numerically simulating the far-field signals from both contained and cratering underground explosions. The numerical simulation techniques represent a synthesis of the finite difference methods for computing ground motion in the near-source large displacement regime and the efficient wave propagation techniques of theoretical seismology.

During the third three-month period of our present contract, our research has been conducted in a number of areas. These areas and the major results obtained in each are summarized in the following paragraphs.

A considerable amount of effort has been directed to the study of explosion generated surface waves during this quarter. Our objective is to understand the dependence of surface wave amplitude on explosion yield, the characteristics of the emplacement medium and the characteristics of the source-receiver travel path. The most commonly used measure of surface wave amplitude is M_s and we have studied the M_s data compiled by others. However, we have also developed our own data base for the Nevada Test Site (NTS) using Airy phase measurements from the WWSSN stations ALQ and TUC. These stations are within 1000 km of NTS and have the advantage of recording events over a large yield range. For events in

common, we find the relative amplitudes from ALQ and TUC to be consistent with the best M_s data.

Comparing events in different local materials at NTS, we find that the M_s coupling is about 0.1 to 0.3 units higher for events below the water table at Pahute Mesa than for comparable events at Yucca Flat. While there are only a few events above the water table at Pahute Mesa, they clearly couple more weakly into M_s than those in the saturated materials. The lowest coupling events in our population are those in dry tuffs at Yucca Flat. While the scatter is considerable, these events are 0.5 to 0.6 units lower, on the average, than saturated events at Yucca Flat. The saturated tuff events in the tunnel beds at Rainier Mesa seem to couple about the same as the saturated tuff events at Yucca Flat. Finally, the PILEDRIVER explosion in granite seems to couple a small amount higher than events in the highest coupling population, the Pahute Mesa explosions below the water table.

Theoretical studies of surface wave generation and propagation are of considerable value for organizing and understanding the empirical data. It is important, therefore, to carefully set forth the theoretical results, making clear the assumptions being made and organizing these results in the proper context for comparing with data. As most commonly used for explosion studies, the theory assumes a spherically symmetric point source representation for the source and a plane-layered model for the path. This theory is fine as far as it goes, but as we study surface waves more closely, certain limitations become apparent. Among the most important of these is the need to account for the fact that the explosion source is certainly more complex than a spherically symmetric point source. It is also important to account for the fact that the crustal structure in the source vicinity where the surface waves are originally excited is often rather different than that for the rest of the path which

controls the dispersion. Making a few reasonable assumptions, our theoretical formulation can be adjusted to account for these limitations.

The surface wave amplitude-yield relationship is controlled by several interlocking effects. Explosion yield changes are almost always accompanied by changes in the burial depth and the properties of the emplacement material. In turn, the burial depth has two separate effects; one due to the changing overburden pressure influence on the source function and one due to the depth effect on surface wave excitation. If the latter effect is isolated, we find that surface wave excitation is a slightly increasing function of depth. That is, if all other factors were fixed, M_s-log yield curves would have a slope of about 1.06 for NTS tuff and slightly greater than unity for NTS granite. Of course, all other factors are not equal, but these too can be isolated to determine their relative influence.

If we assume a spherically symmetric point source representation for the explosion, we find surface wave amplitude to be strongly dependent on the local shear modulus. In fact, we find $M_s \approx \log [\mu^{3/4} \Psi_\infty]$, where Ψ_∞ is the (equivalent elastic) source which is found to be nearly independent of period for periods near those at which M_s is measured. But we know the source is not spherically symmetric. In fact, it is easy to argue that the spherical source for waves traveling upward from the source is different from that for waves traveling downward. How different we do not yet know, though the question is under study.

In studying the relative contribution of the up and downgoing portions of the wave field to teleseismic surface waves, it is interesting to contrast two types of source regions. In one the source is in a soft material like tuff which overlays the hard basement materials. In the second the harder materials (granites) extend nearly to the surface

and this soft rock-hard rock contrast below the source is absent. For the latter case the surface waves from the up and downgoing portions of the source are in phase and add. However, when the sharp contrast is present, the up and downgoing generated surface waves are out of phase and tend to cancel. One interesting result is then that if the upgoing waves were entirely suppressed or scattered, the dependence of teleseismic surface wave amplitude on μ is much reduced.

In addition to the work on surface waves that is briefly summarized in the previous paragraphs, we have been working with deconvolution techniques for analyzing short period body wave recordings of explosions. Teleseismic body wave recordings can be viewed as recordings of the source generated waves modified by a series of transfer functions. There are many combinations of events and/or recordings that allow isolation of one or more of these transfer functions. Once they are known, they can be deconvolved from recordings of future events to isolate the contribution of the source.

A signal deconvolution technique based on "homomorphic deconvolution" methods described in the literature has been programmed and is being tested on data. The success of the technique must really be judged on the transfer functions it gives and, particularly, on how stationary they are from experiment-to-experiment.

II. INTRODUCTION

The primary objective of the research program is to systematically examine the parameters that control magnitude-yield relationships for underground nuclear explosions. During the third three-month period of this contract research has been conducted in the following areas:

1. A review of the dependence of observed surface wave amplitudes on explosion yield and the characteristics of the emplacement material (summarized in Section III).

2. A theoretical study of the dependence of surface wave amplitude on explosion yield, the characteristics of the emplacement material and the characteristics of the travel path (summarized in Section IV).

3. Development and testing of a deconvolution technique for analyzing short period teleseismic recordings of explosions (summarized in Section V).

The remainder of the report is devoted to technical discussions of results in these three areas.

III. SURFACE WAVE OBSERVATIONS

3.1 INTRODUCTION

We wish to understand the dependence of surface wave amplitude on explosion yield and the characteristics of the emplacement medium. The surface wave amplitude data we are using come from two sources. First, there are the M_s data given by Eisenhauer [1976]. Second, we have Airy phase or maximum amplitude measurements from two WWSSN stations at less than 1000 km from NTS. In this section we first summarize these data and then compare them.

The reason for using the Airy phase data is to attempt to extend the surface wave data base to as many different testing areas as possible. We would like to be able to estimate the relative surface wave coupling of events above the water table and at Rainier Mesa compared to the Pahute Mesa and Yucca Flat events below the water table. There are insufficient M_s data for this purpose.

3.2 M_s

The most reliable data for M_s seem to be those compiled by Eisenhauer [1976]. The data of interest for our purposes are those for NTS explosions at or below the water table or in granite. Only a single event (PILEDRIVER) falls in the latter category. The other events are separated according to whether they were at Pahute Mesa or Yucca Flat. Linear least squares equations of the form $M_s = a + b \log W$ were computed for each of the two populations. The results are:

$$\begin{aligned} &\text{Pahute Mesa:} \quad M_s = 1.07 \log W + 1.88, \\ &\text{Yucca Flat:} \quad M_s = 1.08 \log W + 1.70. \end{aligned} \tag{1}$$

Since yields near 150 kt are of primary interest, intercepts for an equation of the form $M_s = a + \log W$ were derived for each test area using explosions between 60 and 415 kt. There were 14 events in the reduced Pahute Mesa population and 21 explosions at Yucca Flat in this yield range. Assuming this unit slope relationship, values of the intercept (a) can be computed for each event. If we average these values we find the following (σ is the standard deviation):

Pahute Mesa: Intercept = 2.00, σ = 0.14,

Yucca Flat: Intercept = 1.87, σ = 0.13, (2)

PILEDRIVER: Intercept = 2.09.

Another useful way to present the "average" M_s for each testing area is by computing the value for a 150 kt event.

	Equation (1)	Equation (2)
Pahute Mesa:	4.21	4.18 $\pm$ 0.14
Yucca Flat:	4.05	4.05 $\pm$ 0.13
PILEDRIVER:	4.26	4.26

3.3 AIRY PHASE AMPLITUDE FROM WWSSN STATIONS ALQ AND TUC

Data from the WWSSN stations ALQ and TUC were collected for a large sampling of NTS explosions. Some results were reported by Bache, et al., [1975a]. The station distances and azimuths are summarized below:

	ALQ		TUC	
Test Area	Distance (km)	Azimuth	Distance (km)	Azimuth
Yucca Flat	900	103°	720	136°
Rainier Mesa	910	103°	730	136°
Pahute Mesa	930	103°	755	135°
PILEDRIVER	900	104°	730	137°

These values are for events near the center of each test area. Typical seismograms for these two stations are shown in Figure 1.

The peak-to-peak amplitudes of the maximum cycle in the Rayleigh wave train and the period of that cycle were measured for each event. All measurements were from the vertical component. Since the propagation path lies entirely in a continental structure and the instrument passband is 7 to 30 seconds, the maximum amplitude is associated with the Airy phase. The period of this phase was 11.5 $\pm$ 0.5 seconds at ALQ and 8 $\pm$ 0.5 seconds at TUC. A striking characteristic of the data was the similarity of the waveforms from event-to-event at each station. Thus, the amplitude measurements consistently sample the same portion of the waveform.

The Airy phase amplitudes were converted to M_s values by using the formulas:

$$\text{ALQ:}\quad M_s^A = \log A + 2.72,$$
$$\text{TUC:}\quad M_s^T = \log A + 2.17. \qquad (3)$$

The constant factors in these equations were chosen to make M_s^A and M_s^T be about the same, on the average, as Eisenhauer's M_s. No other meaning is attributed to them.

The ALQ and TUC M_s values may be analyzed in about the same way as were the M_s data in Section 2.2. First, the two

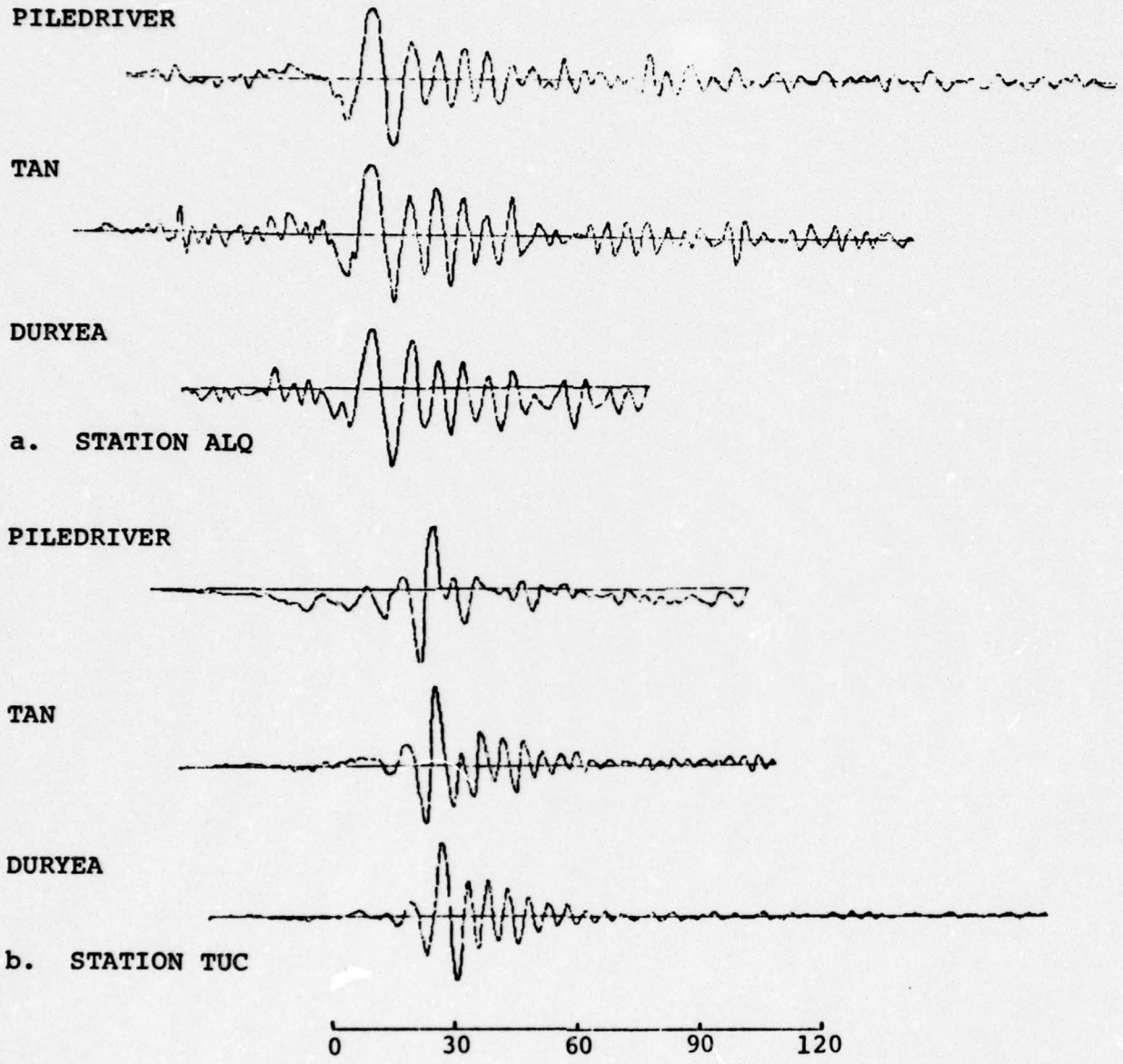

Figure 1. Long period vertical component recordings of three NTS explosions at two WWSSN stations.

measurements are averaged to obtain our best estimate of M_s from these Airy phase data. We then separate the data by test area and compute a linear least square fit to each population. The regression is done assuming the yield values are exact and the standard deviation of the M_s values from the mean is determined. The linear best-fit equations for each population together with the standard deviations are as follows (the number of events is listed in parentheses):

Pahute Mesa below the water table (9):
$M_s = 0.86 \log W + B, \qquad \sigma = 0.09,$

Yucca Flat below the water table (30):
$M_s = 1.17 \log W + B - 0.93, \ \sigma = 0.19,$

Pahute Mesa above the water table (3):
$M_s = 1.21 \log W + B - 1.09, \ \sigma = 0.05,$ (4)

Yucca Flat above the water table (15):
$M_s = 0.78 \log W + B - 0.82, \ \sigma = 0.27,$

Rainier Mesa, tunnel shots only (10):
$M_s = 0.77 \log W + B - 0.41, \ \sigma = 0.19.$

The M_s data together with the least square fitting lines are plotted in Figure 2. As expected from the large σ values in (4), there is considerable scatter in the data, especially for the Yucca Flat events.

How well do the Airy phase data correlate with the Eisenhauer M_s estimates? For saturated events at Pahute Mesa there are seven events for which both data are available. For Yucca Flat there are eleven common events. In Figure 3 the Airy phase M_s estimates from Figure 2 are plotted versus Eisenhauer's M_s for the common events. While there is some scatter, we see that the two M_s estimates are consistent. Taking the residuals (M_s [Eisenhauer] - M_s [ALQ + TUC]) and

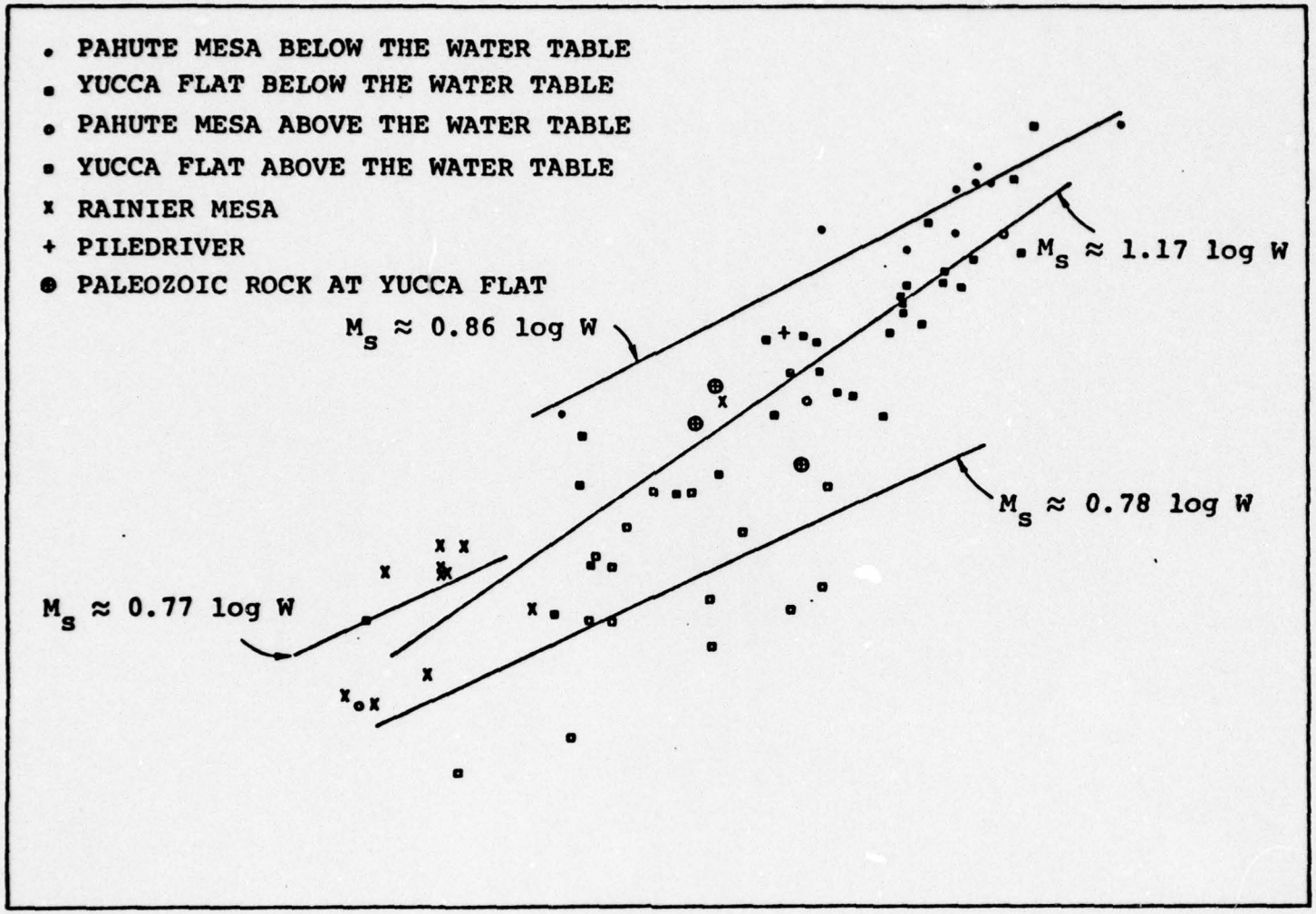

Figure 2. The M_S values from the WWSSN stations ALQ and TUC are plotted versus explosion yield. The explosions are divided into different populations according to the gross properties of the emplacement media.

averaging, we find the mean to be 0.04 with a standard deviation of 0.10 M_s units. For the Pahute Mesa events taken separately, the mean residual is 0.01 and it is 0.06 for the Yucca Flat events. The small mean is really a test of our selection of the constants in (3). The important value is the σ of 0.10.

3.4 THE RELATIVE M_s COUPLING OF EVENTS IN DIFFERENT MATERIALS AT NTS

We are interested in the dependence of surface wave amplitude on explosion yield and on the characteristics of the emplacement medium. We take M_s to be the measure of surface wave amplitude. It is important to recognize that it is generally impossible to entirely separate yield effects from those due to burial depth and local material property variations. While Eisenhauer's Pahute Mesa and Yucca Flat events below the water table seem to be populations for which the local material property variations are minimized, burial depth is directly proportional to yield for most events. Therefore, the M_s - log W curves in (1) also incorporate M_s - depth effects.

The Airy phase data discussed in Section 3.2 were collected to attempt to estimate the relative surface wave coupling for different emplacement materials. Once again, it is impossible to isolate the coupling effects since the yield and depth range are generally different for different source materials. It is necessary to keep this in mind when comparing M_s values from the different test areas.

The M_s data in (1) show M_s - log W to have a slope of about 1.07 for events in saturated tuffs and rhyolites. Considering the scatter, the data of (4) and Figure 2 do not contradict the conclusion that the M_s - log W slope is

one or a bit larger. Further, the results of Figure 3 give confidence that the Airy phase amplitudes can be used to estimate the relative M_s coupling for explosions in different areas.

Eishenhauer computed the average value of M_s - log W for events in a limited yield range (60 to 415 kt) for the Pahute Mesa and Yucca Flat events below the water table. The results were given in (2). We can do the same for each grouping of events discussed in Section 2.3. The results are as follows:

Pahute Mesa below the water table (9 events),
Intercept = 2.06, σ = 0.11.

Yucca Flat below the water table (21 events),
Intercept = 1.78, σ = 0.17.

Pahute Mesa above the water table (3 events),
Intercept = 1.64, σ = 0.17.

Yucca Flat above the water table (15 events),
Intercept = 1.21, σ = 0.28.

Rainier Mesa tunnel explosions (10 events),
Intercept = 1.75, σ = 0.19.

Yucca Flat Paleozoic rock (3 events),
Intercept = 1.69, σ = 0.27

PILEDRIVER:
Intercept = 1.95.

These results together with those from (2) are presented graphically in Figure 4. We see that the M_s and Airy phase data agree that the M_s coupling is about 0.1 to 0.3 units higher for the events below the water table at Pahute Mesa

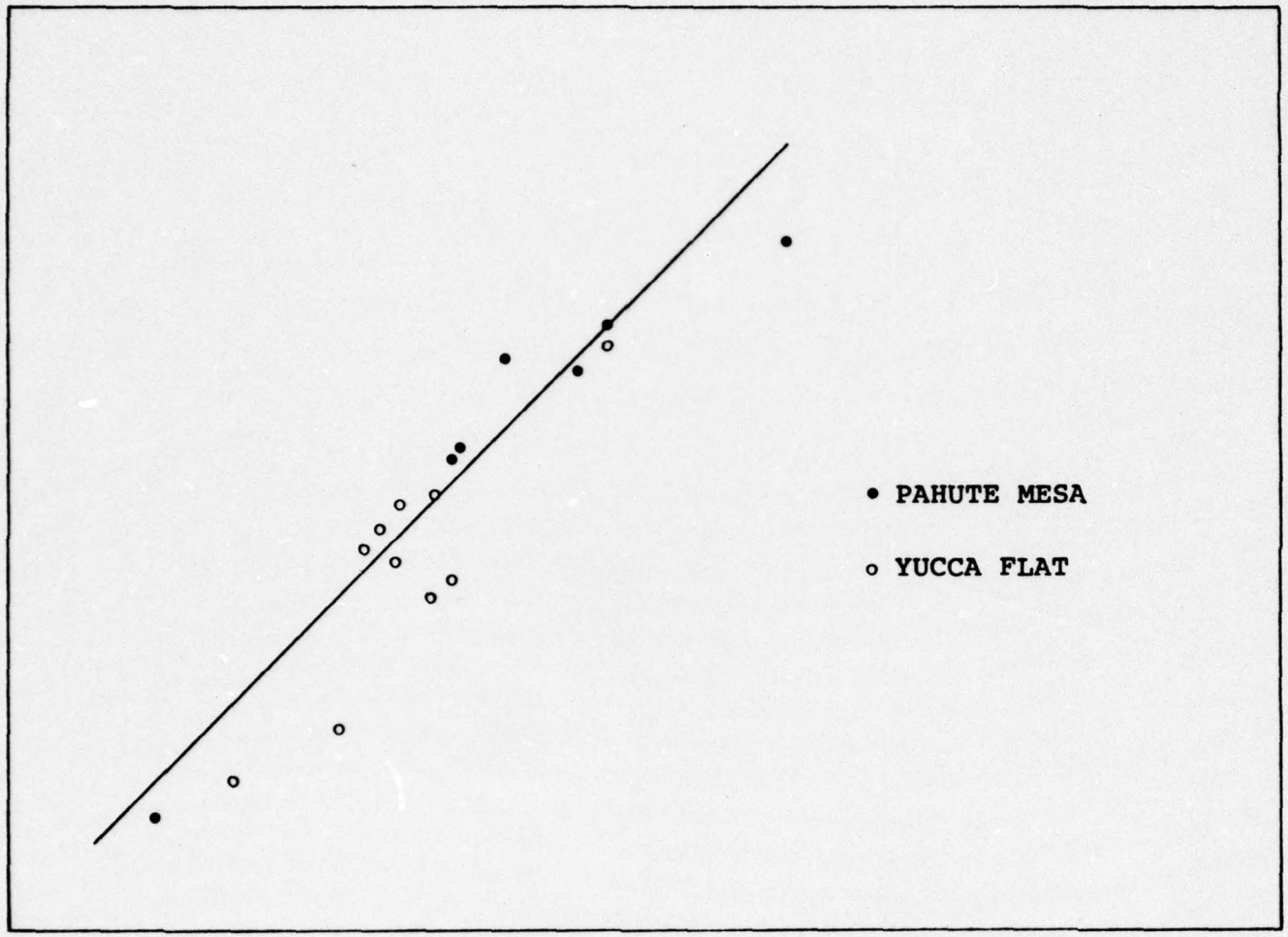

Figure 3. The M_s estimates from ALQ and TUC are compared to those from Eisenhauer [1976] for eighteen common events. A line of unit slope is shown for convenience.

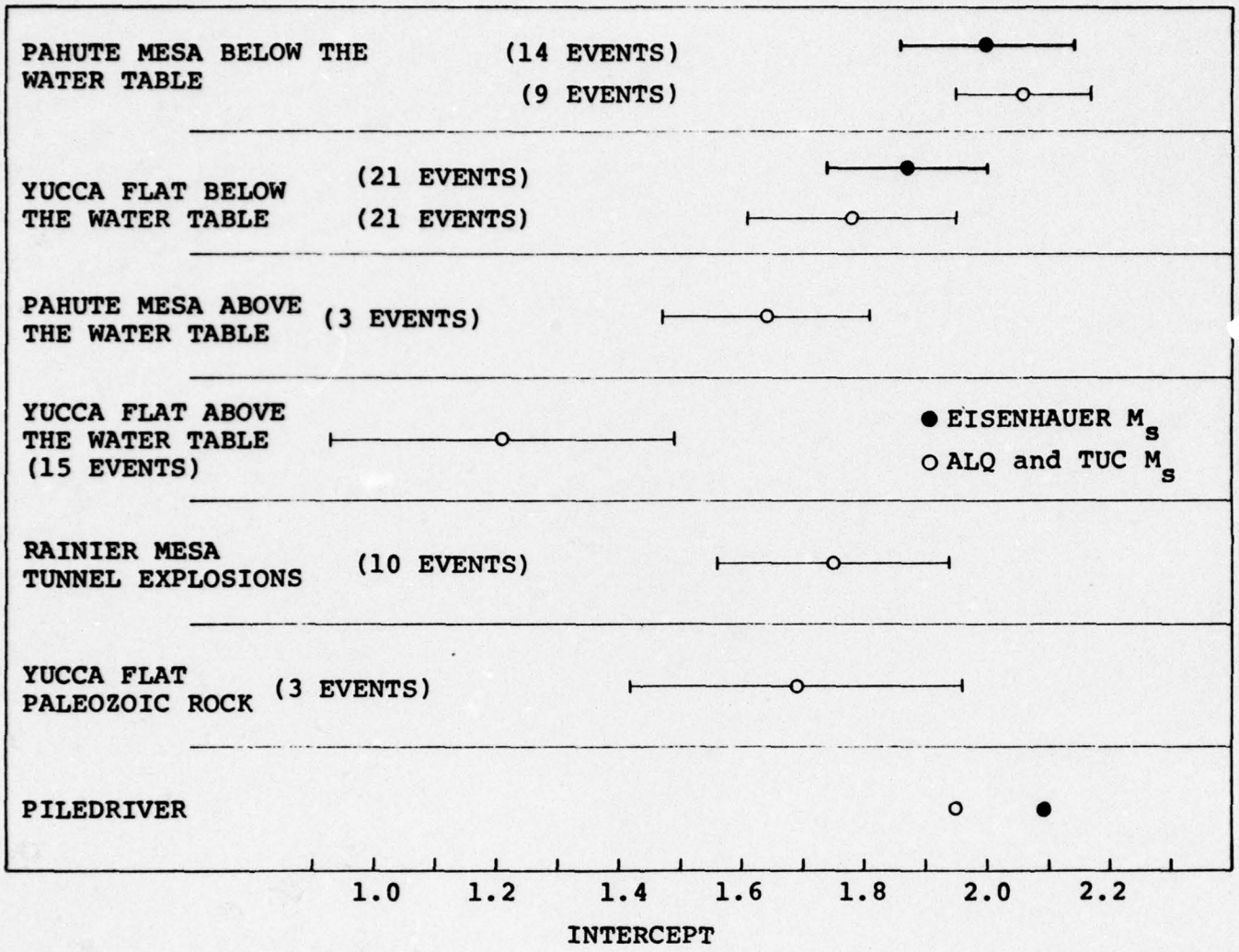

Figure 4. The mean values of M_S-log W for events in a limited yield range in each of the testing areas are depicted by a bar graph. For each data set the lines represent the mean $\pm$ one standard deviation.

than comparable events at Yucca Flat. There are only a few events above the water table at Pahute Mesa, but they clearly couple more weakly into M_s than those in saturated materials. The lowest M_s events are those in dry tuffs at Yucca Flat. The scatter is quite large for these low yield events, but M_s - log W is 0.57 lower, on the average, than for the saturated events at Yucca Flat, a number much larger than the standard deviation of the data. The saturated tuff explosions in the tunnel beds at Rainier Mesa seem to couple about the same as the saturated tuff events at Yucca Flat. The same can be said about the three events identified as being in Paleozoic rock at Yucca Flat. Since these events were detonated 23 meters or less from the tuff-Paleozoic interface [Springer and Kinnaman, 1971], the identification of these events as being in paleozoic rock is somewhat ambiguous and we are probably not seeing the true differences between events in saturated tuff and the paleozoic rocks. Finally, the PILEDRIVER event seems to couple like the highest coupling population, the Pahute Mesa events below the static water table.

IV. THEORETICAL SURFACE WAVE GENERATION BY EXPLOSIONS

4.1 INTRODUCTION

In this section we first outline our procedure for computing theoretical seismograms for underground explosions, making clear the assumptions being made. The theoretical dependence of surface wave amplitude on explosion yield, source depth and properties of the emplacement material is then discussed. We also address the dependence of M_s on properties of the travel path.

4.2 OUTLINE OF THE THEORY

The computational method being used for generating theoretical surface wave seismograms is based on that outlined by Harkrider [1964, 1970]. The formulation of the theory is entirely in terms of linear elasticity. The effect of anelastic attenuation is included via an empirically determined Q operator. The explosion source is, of course, highly nonlinear. For using the surface wave theory it is then necessary to represent this source in terms of an "equivalent elastic source." For spherically symmetric explosions this equivalent elastic source is the reduced displacement potential.

The most elementary application of the theory is to assume that the entire source-receiver travel path can be modeled as a single multilayered medium. The explosion source is assumed to be represented by a reduced displacement potential. A great deal can be learned about explosion generated surface waves from this theoretical formulation, but there are several problems to be addressed. Among these are:

1. Say we were interested in surface waves from NTS to a fixed seismic network. The local geology changes from place to place within NTS, but most of the source-receiver path remains the same. If we are restricted to a single path model, there is no consistent way to deal with explosions in different local media.

2. We know that the explosion is not a spherically symmetric source of elastic waves embedded in one layer of a layered earth. The question is, how severe is the effect of assuming that it is?

3. The previous question carries with it a whole set of subquestions about different aspects of the behavior in the source region. Among the nonspherical effects that are potentially significant for surface wave coupling are:

    a. The nonlinear region intersects the free surface for most events. The theory assumes elastic reflection by the free surface.

    b. Some form of tectonic stress release is thought to be associated with many large underground explosions (e.g., Archambeau and Sammis [1970]; Toksöz and Kehrer [1972].

    c. We know the source material is not homogeneous in the large nonlinear region associated with underground nuclear explosions. As a simple

example, the overburden pressure changes significantly from top to bottom of this region.

In the remainder of this section we first outline the elementary theory and then the modifications employed to deal with the first problem listed above. The second and third problems are addressed, at least in a tentative way, in later sections, particularly Section 4.6.

Assume that the entire travel path is represented by a single multilayered earth model and the source is represented by a reduced displacement potential. Then the Fourier-transformed vertical component of the fundamental mode Rayleigh wave is

$$\hat{w}(r,\omega) = - i\omega 4\pi\mu_s \hat{\Psi}(\omega) \frac{K_s \underset{\sim}{A}_R}{c_R} H_o^{(2)}\left(\frac{\omega r}{c_R}\right) , \tag{5}$$

where $\Psi(\omega)$ is the reduced displacement potential, μ_s is the shear modulus of the source layer, r is epicentral distance and c_R is the phase velocity of the Rayleigh wave component of frequency. The A_R is the amplitude response of the layered medium and is independent of the source depth. The depth excitation factor is K_s which, in the notation of Harkrider [1964], may be written

$$K_s = \frac{\dot{u}_s^*(h)}{\dot{w}_o} - \frac{1}{2\mu_s} \frac{\sigma_s^*(h)}{\dot{w}_o/c_R} , \tag{6}$$

where h is the source depth, $\dot{u}_s^*$ and $\dot{w}_o^*$ are radial and vertical velocities and σ_s^* is the normal stress. The subscripts o and s refer to the free surface and the source layer. The two

terms in (6) are tabulated for several source structures by Harkrider [1970]. To account for anelastic attenuation and sphericity, we multiply (5) by

$$e^{-\gamma r} \left(\frac{r}{a_e \sin\Delta}\right)^{1/2} , \qquad (7)$$

where γ is an empirically determined attenuation factor, Δ is range in degrees and a_e is the radius of the earth.

To use (5) we must have an average earth model for the travel path. This is fine for the dispersion characteristics of the path and numerous seismologists have demonstrated that synthetic seismograms can be computed that look very much like the observed seismograms (from which data, after all, the average earth models are constructed). However, a problem arises when the material in the local source region is not the same as the "average" material at that depth. It is possible to ignore this problem (and many people have) if one is dealing with a series of events in, more-or-less, the same source material. For example, one could construct theoretical M_s-log yield curves for explosions in any of the different NTS source materials discussed in Section II. However, the problem is impossible to ignore if one is attempting to compare events in close proximity, but in different source materials.

This problem of different source materials, same average path is one that has interested us for some time. An earlier attempt to deal with the difficulty was to continue to use a single path model, but to let the source region be modeled by a spherical plug of the source material. A modified reduced displacement potential incorporating the effect of the boundary between the "source" and "global" materials is then used. This theory was worked out and the consequences were explored to some degree by Harkrider and Bache

and the results were reported by Bache, et. al., [1975b]. While the results are interesting, this method for handling the source region is not very satisfactory. The method we now prefer is described in subsequent paragraphs.

A natural way to approximate the different source region, common average path situation is with two earth models, one for the source region and one for the remainder of the path. For this we must be able to account for propagation of Rayleigh waves across the boundary between the two. Alewine [1974] gives a correction to account for the boundary that is based on the work of McGarr [1969] and McGarr and Alsop [1967]. Letting the source and receiver portions of the path be denoted by subscripts 1 and 2, the equation for mixed path Rayleigh waves according to these authors is:

$$\hat{w} = - i\omega 4\pi\mu_s \hat{\Psi} \frac{K_{s_1} \underset{\sim}{A}_{R_1}}{c_{R_1}} T(\omega) H_o^{(2)}\left(\frac{\omega r_1}{c_{R_1}} + \frac{\omega r_2}{c_{R_2}}\right) \exp(-\gamma_1 r_1 - \gamma_2 r_2)$$

$$\cdot \left(\frac{r_1 + r_2}{a_e \sin(\Delta_1 + \Delta_2)}\right)^{1/2} . \qquad (8)$$

The transmission coefficient, $T(\omega)$, is derived by assuming the total horizontal energy flux remains constant during the transmission of the Rayleigh wave across the boundary. The coefficient is given by

$$T(\omega) = \left(\frac{E_1 U_1}{E_2 U_2}\right)^{1/2} , \qquad (9)$$

where U is the group velocity and E is the total potential or kinetic energy normalized to ω_o, the surface vertical displacement. In using this coefficient we assume that there is

little or no mode conversion at the boundary and that the boundary is far enough from the source so that the wave front has small lateral curvature. Finally, since no refraction effects are included, we assume that the wave front is parallel to the boundary.

How do we use (8) to study NTS explosions? First, as far as we know, the only difference in source structure between events in different portions of NTS is in the top few kilometers of the structure. We need the freedom to change this portion from granite to tuff or some other material. Then for the long periods of interest for M_s, the boundary is nearly transparent and $T(\omega) \approx 1$. Even at short periods it seems reasonable to let $r_1 \to 0$ because the dispersion and attenuation are average path quantities that, to the extent they are derived from NTS data, already incorporate any mixed path effects that might be present.

As far as the longer period surface waves and M_s are concerned, the practical consequences of using this formulation are simple and attractive. The depth excitation factor, K_s, is computed using a structure that has the correct material at the source depth. There is then no ambiguity in the use of μ_s. That is, the material for Ψ is the same as the material in the multilayered model at the source depth. The dispersion properties that control the far-field waveform are controlled by the "global" model for the rest of the path.

The points made in the previous paragraphs will now be clarified by considering an example. As an average path model we will use the western United States model 35-CM2 proposed by Alexander [1963], which is tabulated in Table 1. For the source region we use the same model modified to account for details of the local geology. Two examples will be considered. In one the source is in granite like PILEDRIVER and the second

TABLE 1

CRUSTAL MODEL 35-CM2 FROM ALEXANDER [1963]

Layer	Depth (km)	Thickness (km)	α (km/sec)	β (km/sec)	ρ (gm/cm^3)
1	2.0	2.0	3.8	1.75	2.2
2	15.0	13.0	6.1	3.6	2.8
3	25.0	10.0	6.2	3.7	2.8
4	35.0	10.0	7.7	4.1	3.25
5	48.7	13.7	8.1	4.65	3.4
6	64.0	15.3	7.95	4.55	3.45
7	83.0	19.0	7.85	4.5	3.45
8	103.5	20.5	7.8	4.4	3.45
	CRUSTAL MODEL 35-CM2 WITH A PILEDRIVER GRANITE CAP				
1	0.06	0.06	1.44	0.83	1.5
2	0.2	0.14	4.69	2.71	2.45
3	2.0	1.8	5.33	2.78	2.67
4-9	Layers 2-8 of 35-CM2				
	CRUSTAL MODEL 35-CM2 WITH YUCCA FLAT TUFF CAP				
1	0.15	0.15	1.2	0.8	1.7
2	0.20	0.05	1.8	1.0	1.78
3	2.0	1.8	2.35	1.3	1.86
4-9	Layers 2-8 of 35-CM2				

source area is Yucca Flat. The two source structures are also tabulated in Table 1. The only differences between the three structures are in the top two kilometers.

The quantities characterizing mixed path models made up of the two source region models and the average path model of Table 1 are plotted in Figures 5, 6 and 7. The phase and group velocities for the three structures are shown in Figure 5. The amplification factor A_R is plotted in Figure 6. In Figure 7 is plotted the depth excitation factor, K_s, for the two source region models and the transmission coefficient, T, for the boundaries. From Figures 5 and 6 we see that the differing material in the top two kilometers causes substantial differences in the quantities plotted for periods below 10 to 15 seconds. The same is true of the depth excitation factor in Figure 7. However, the transmission coefficient is within 20 percent of unity for periods down to eight seconds.

The important result illustrated by the foregoing examples is that the long periods at which M_s is measured pass essentially unchanged through material boundaries that are restricted to the top few kilometers of the models. This provides a convincing justification for computing surface waves according to the formula

$$\hat{w} = i\omega 4\pi\mu_s \hat{\Psi} \frac{K_{s_1} \underset{\sim}{A}_{R_1}}{c_{R_1}} T(\omega)\ H_o^{(2)}\left(\frac{\omega r}{c_{R_2}}\right) e^{-\gamma r} \left(\frac{r}{a_e \sin\Delta}\right), \quad (10)$$

where r is the range and the subscripted quantities are as in (8). This procedure allows us to use a single average path model for events in a particular source region while accounting for changes in the very local material properties in a consistent way.

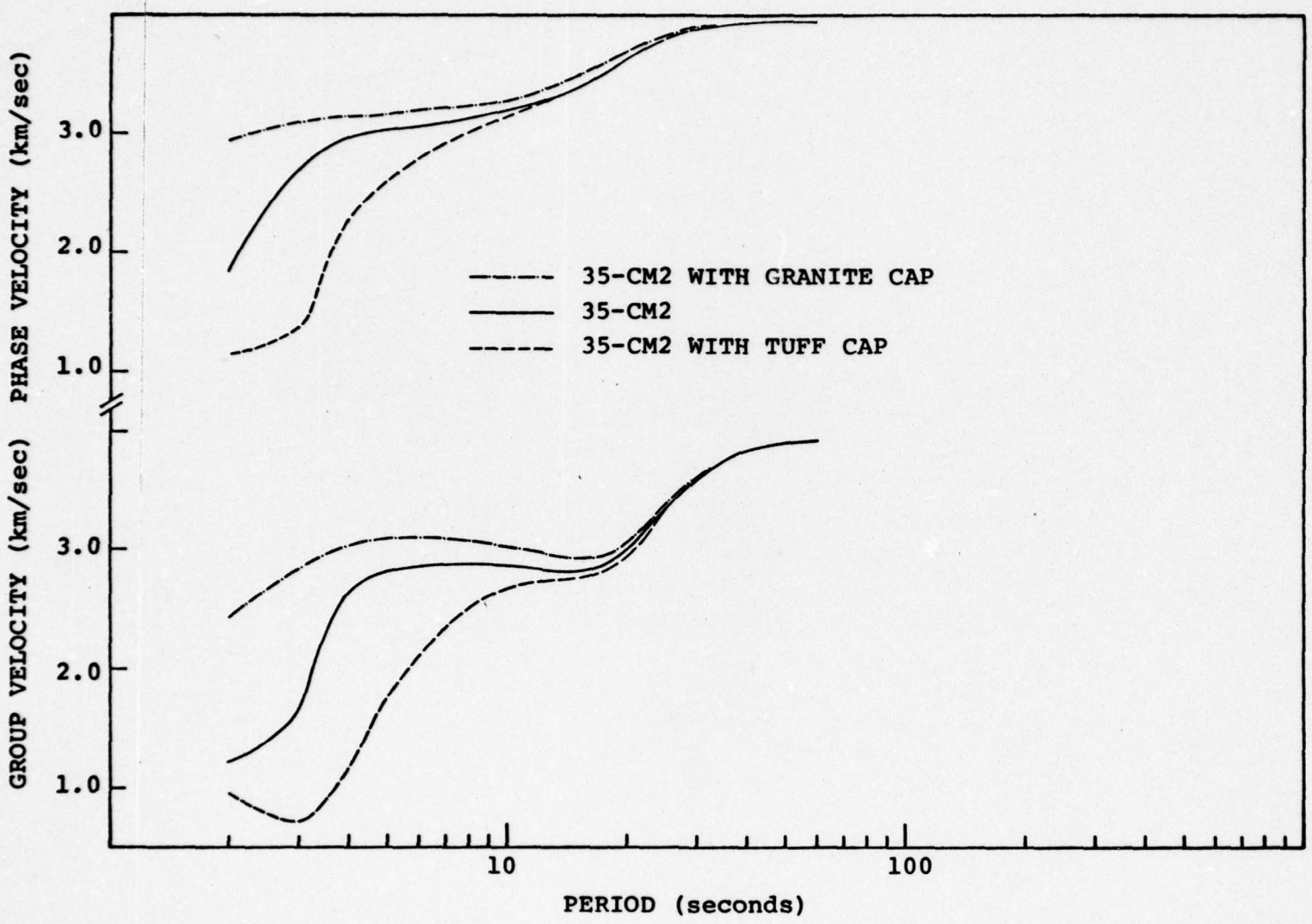

Figure 5. The phase and group velocities are plotted versus period for the three crustal models of Table 1.

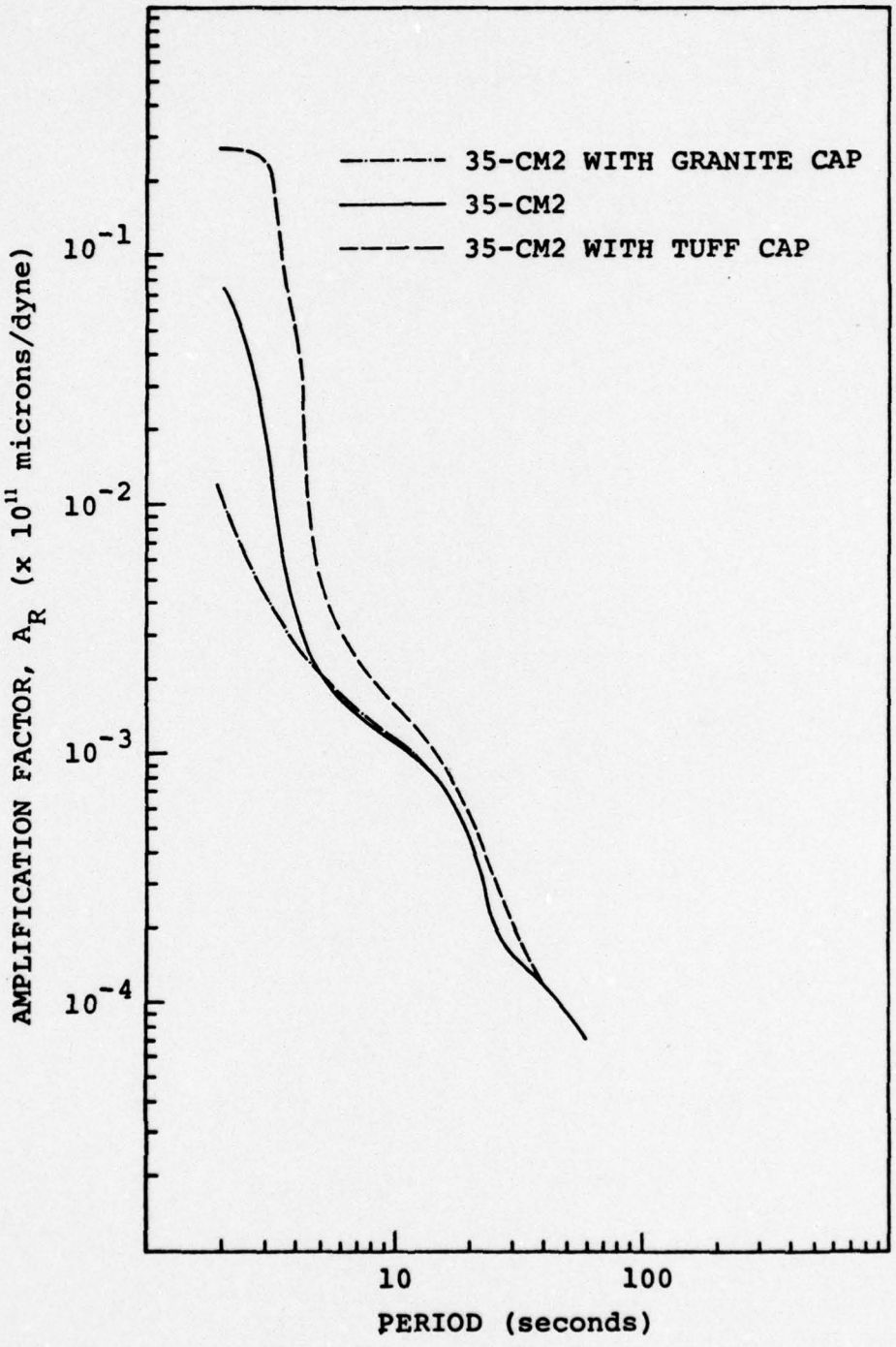

Figure 6. The amplification factor is plotted versus period for the structure of Table 1.

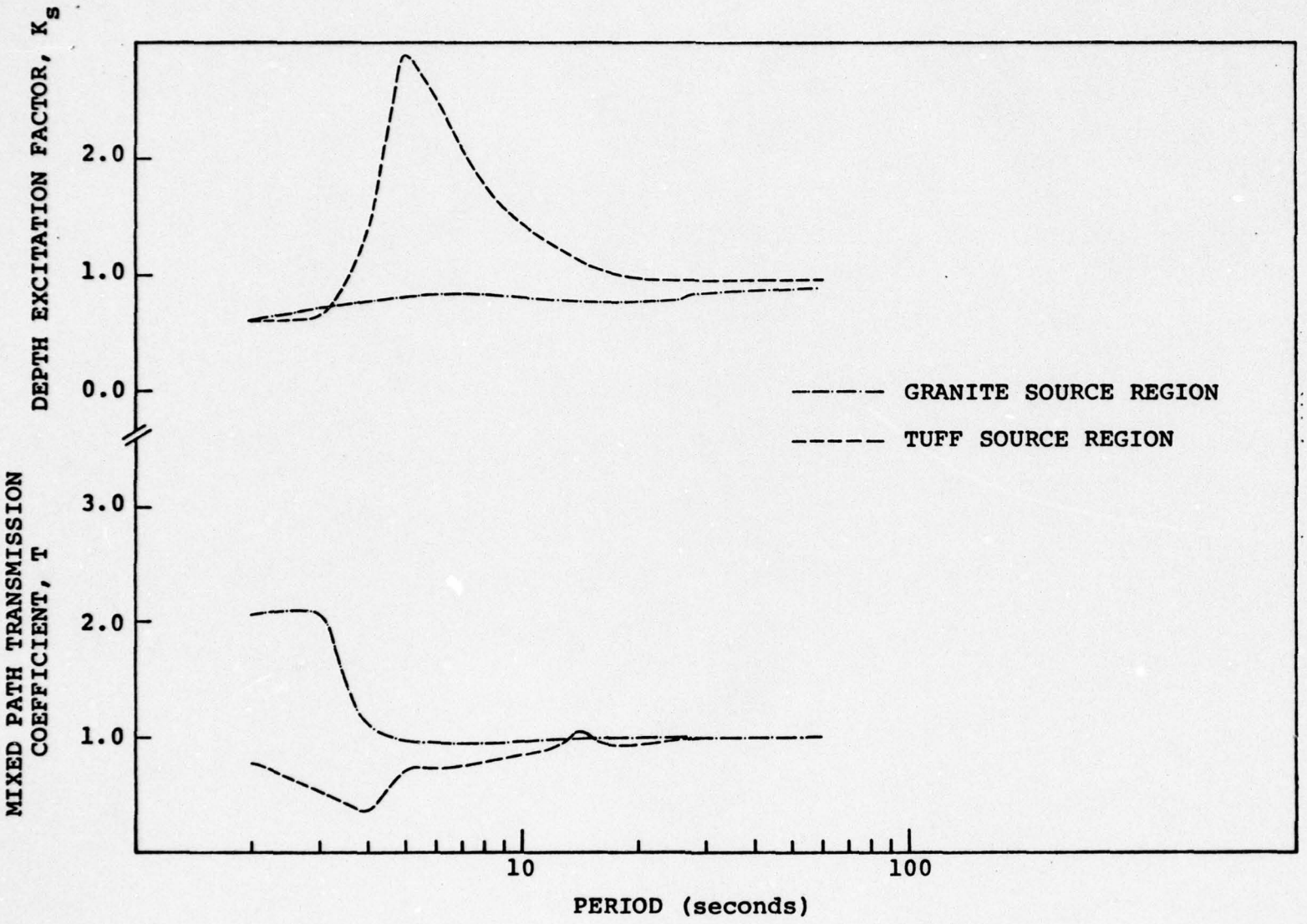

Figure 7. The transmission coefficient and depth excitation factor are plotted versus period for two mixed path models.

4.3 THEORETICAL SURFACE WAVE AMPLITUDE - YIELD RELATIONSHIP

Using the theoretical results of the previous section, theoretical amplitude-yield curves are constructed for explosions in different source materials. The burial depth was assumed to vary according to 107 $W^{1/3}$ (meters). Two sets of theoretical seismograms were computed, one for explosions in granite and one for explosions in a material similar to the saturated tuffs at Yucca Flat. The travel path models were those discussed in Section 4.2 as examples of the mixed path technique. They are tabulated in Table 1. The attenuation model is that of Tryggvason [1965] and the instrument response is for the standard LRSM long period system.

The theoretical seismograms are shown in Figures 8 and 9. On each record is shown the depth of burial and yield of the source. These seismograms are for a range of 3000 km. For the periods appearing on the records of Figures 8 and 9 the source function ($\dot{\Psi}[\omega]$) is essentially constant for materials of interest. Therefore, the only important characteristic of the source potential is its static level or Ψ_∞ and the seismograms scale with this quantity. For convenient comparison, all theoretical seismograms of this section were computed with the same source function which is characterized by $\Psi_\infty = 9.1\ m^3$ at a yield of 0.02 kt.

From the seismograms of Figures 8 and 9 we see that variations in yield and burial depth have no effect on the teleseismic wave form. Comparing the two sets, it is clear that changing the source material has only a very minor effect. Therefore, it is easy to make consistent measurements for computing M_s. The cycle at which amplitude measurement is made is indicated on each record along with the M_s which is computed from

$$M_s = \log \frac{A}{20} + \log \Delta + 1.12 \ , \qquad (11)$$

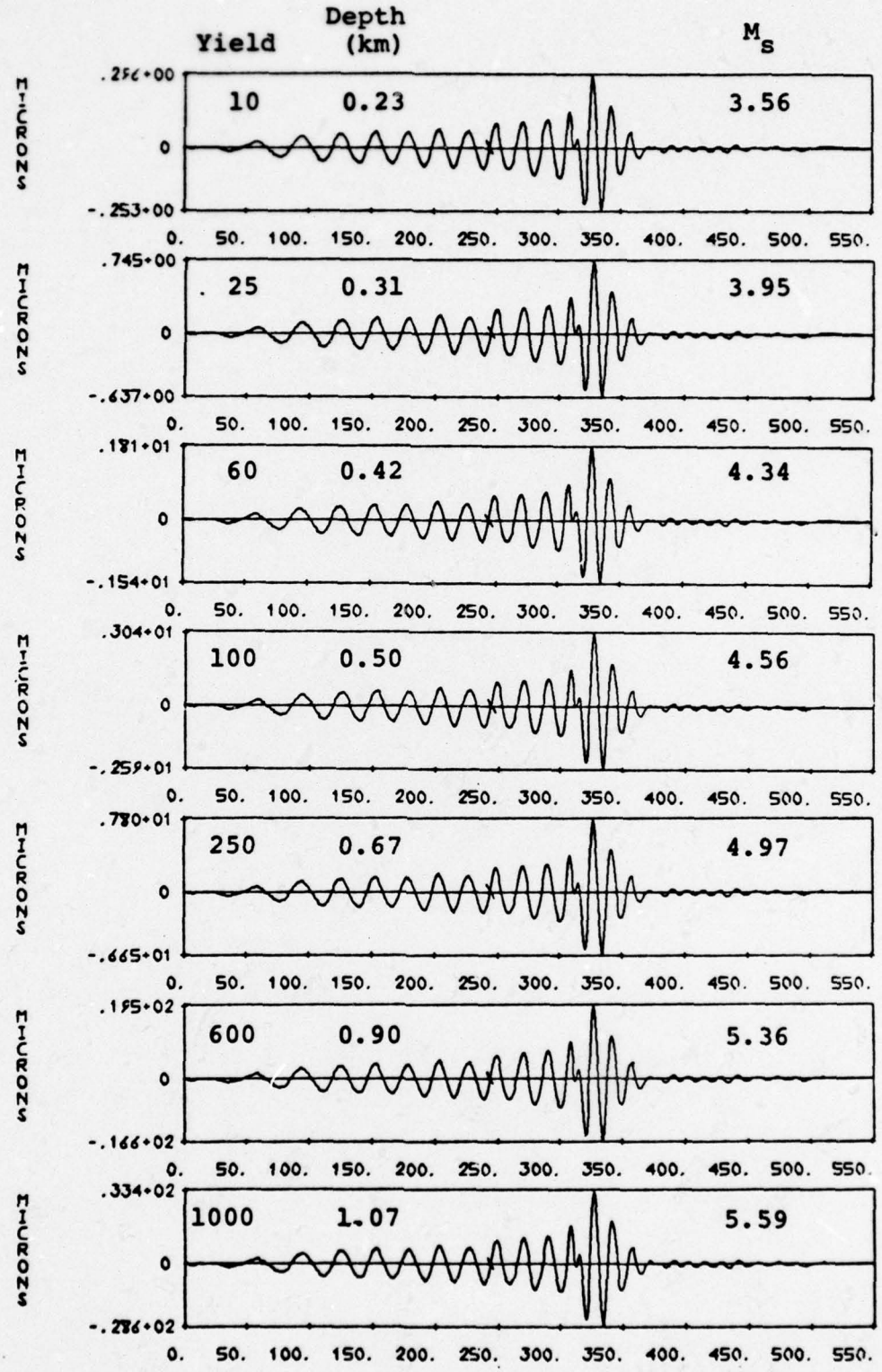

Figure 8. Theoretical seismograms are shown for a series of explosions in NTS granite. The yield, burial depth and M_s are shown with each record and the cycle at which M_s is measured is indicated with a bar. The period of this cycle is 19.7 seconds. Positive vertical is down.

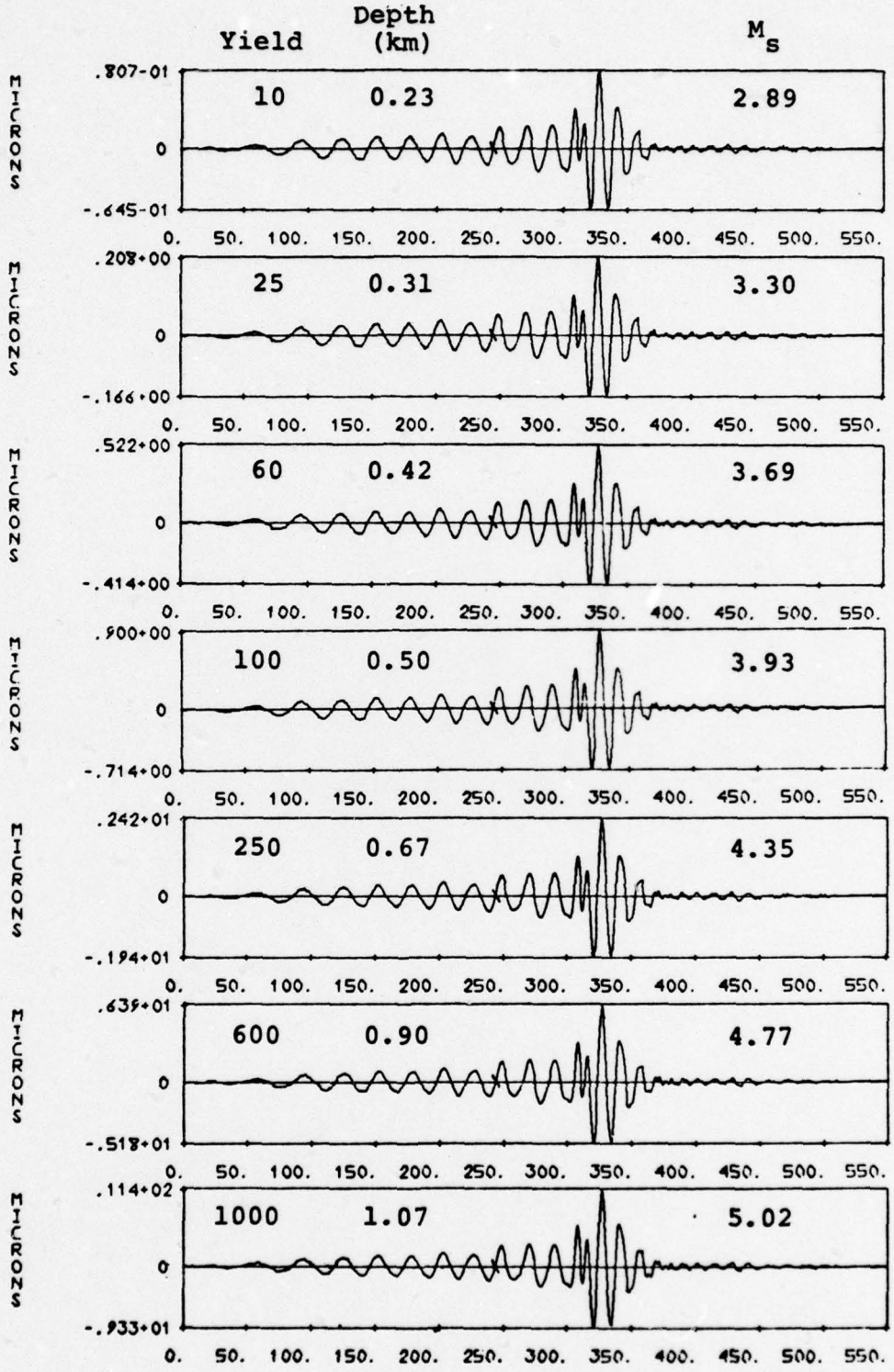

Figure 9. Theoretical seismograms like those in Figure 8 except the source is in tuff. The period of the M_s cycle is 18.8 seconds.

where A is peak-to-peak amplitude in nanometers and Δ is range in degrees. This is the formula used by Eisenhauer [1976].

The M_s values from Figures 8 and 9 are plotted versus yield in Figure 10. A linear least square fit was made to each data set and the results are indicated in the figure. The first thing to be noticed is that the slope is slightly greater than unity. Referring to (10), the only quantities that change from one yield to another are the source function (Ψ), which is assumed to cube-root scale with yield, and the depth function K_{s1}. The values of K_{s1} at 20 seconds are plotted in Figure 11 for the two cases. We see that for the granite source region the depth function is nearly constant over this range. The slope of 1.02 is then due to the source excitation at 20 seconds increasing slightly over the 10 to 1000 kt yield range. The greater slope of 1.06 for the tuff source region is due to the fact that the K_{s1} increases somewhat with depth. For example, with all other factors being equal, an explosion in tuff at a depth of 1.07 km will have an M_s that is 0.08 units higher than one at a depth of 0.23 km.

The second interesting feature of the seismograms of Figures 8 and 9 is the variation of amplitude with the source material while the source function (Ψ) is held fixed. From (10) we see that the spectral amplitude ratio is

$$\frac{\omega^{(G)}}{\omega^{(T)}} = \frac{\mu_s^{(G)}}{\mu_s^{(T)}} \frac{K_{s_1}^{(G)}}{K_{s_1}^{(T)}} \frac{C_{R_1}^{(T)}}{C_{R_1}^{(G)}} \frac{T_{(\omega)}^{(G)}}{T_{(\omega)}^{(T)}} \frac{A_{R_1}^{(G)}}{A_{R_1}^{(T)}}, \qquad (12)$$

where the superscripts indicate whether the source is in granite (G) or tuff(T). These quantities are plotted in Figures 5, 6, and 7 or tabulated in Table 1. We find that

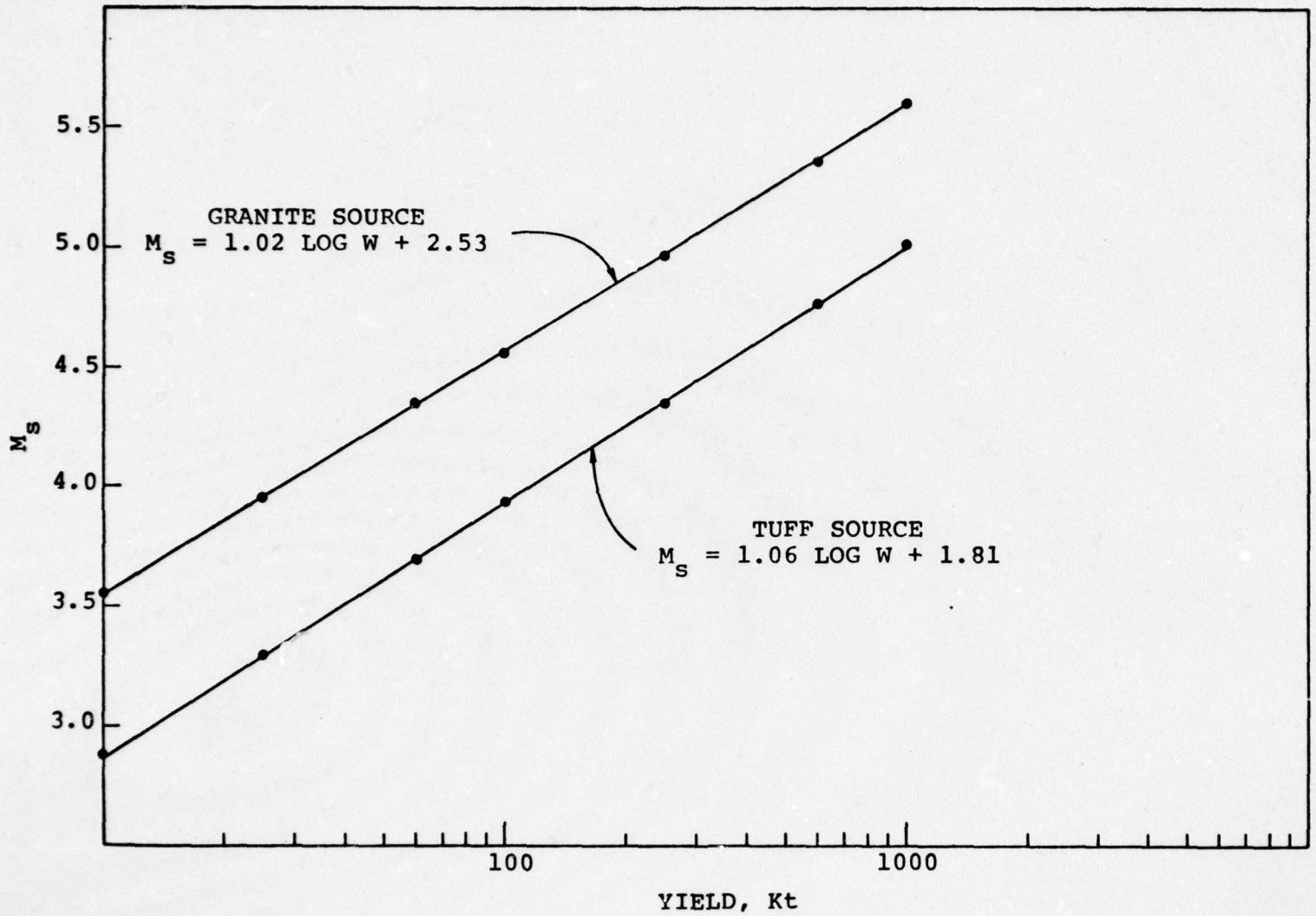

Figure 10. The M_s values from Figures 8 and 9 are plotted versus yield and are fit by a linear least squares regression, assuming all error is in M_s.

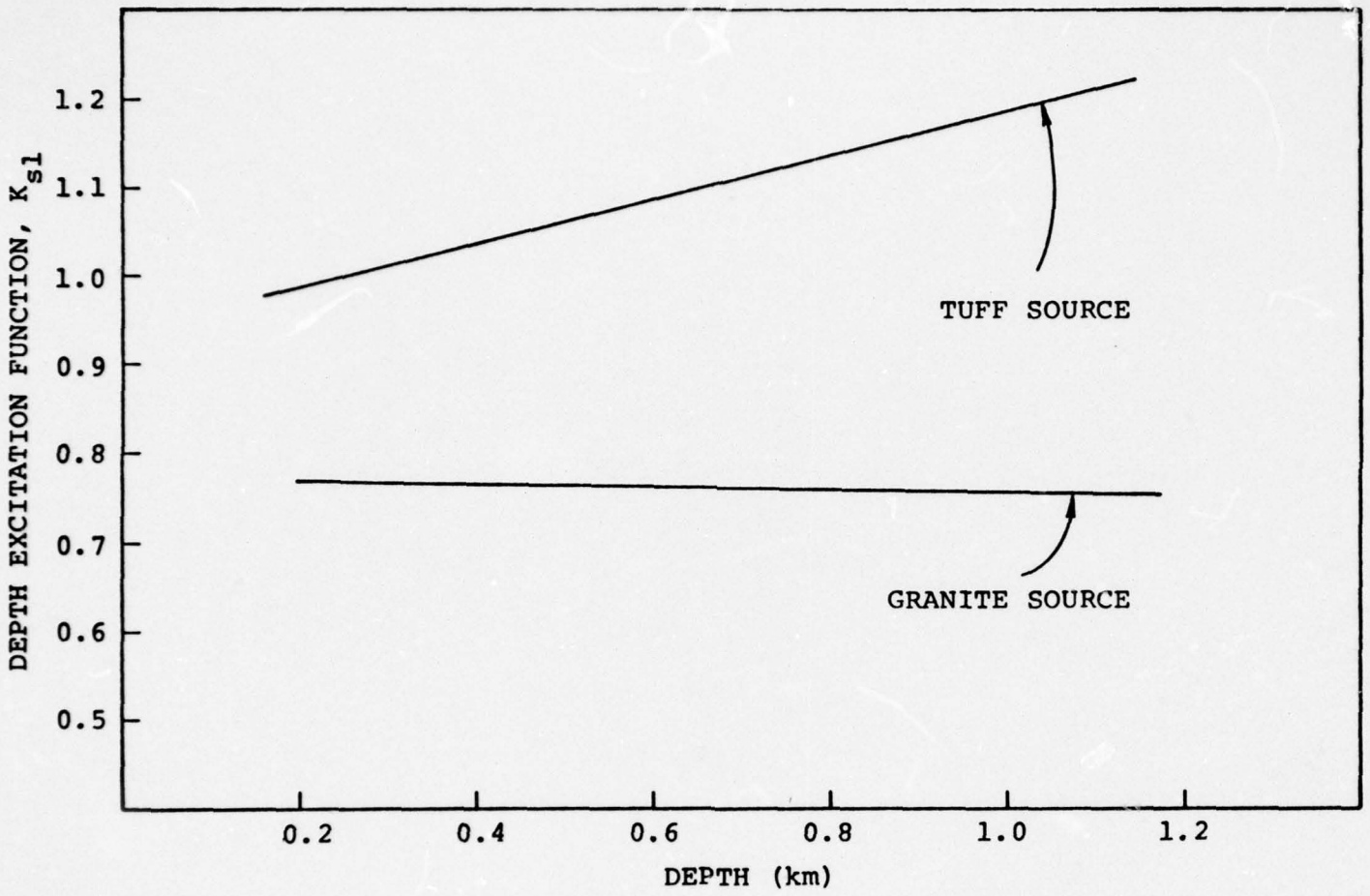

Figure 11. The depth excitation factor, K_{s1}, at 20 seconds period is plotted versus depth for the tuff and granite source regions.

$$\frac{C_{R_1}^{(T)}}{C_{R_1}^{(G)}} \cdot \frac{T_{(\omega)}^{(G)}}{T_{(\omega)}^{(T)}} \cdot \frac{\underset{\sim}{A}_{R_1}^{(G)}}{\underset{\sim}{A}_{R_1}^{(T)}} = 0.93 \ , \tag{13}$$

and, therefore, these factors are not very significant. Then, to a good approximation,

$$\frac{\hat{w}^{(G)}}{\hat{w}^{(T)}} \approx \frac{\mu_s^{(G)} K_{s_1}^{(G)}}{\mu_s^{(T)} K_{s_1}^{(T)}} \frac{\hat{\dot{\Psi}}^{(G)}}{\hat{\dot{\Psi}}^{(T)}} \ , \tag{14}$$

where we have introduced the source functions which, in general, are important for the scaling. Referring to the definition of K_s (6), we see that μ_s plays an important role in this parameter. In view of this fact, we find it useful to fit the amplitude ratio by the relationship

$$\frac{\hat{w}^{(G)}}{\hat{w}^{(T)}} \approx \left(\frac{\mu_s^{(G)}}{\mu_s^{T}} \right)^n \frac{\hat{\dot{\Psi}}^{(G)}}{\hat{\dot{\Psi}}^{(T)}} \ . \tag{15}$$

For the example treated here the n varies from 0.83 at 10 kt to 0.71 at 1000 kt. At 150 kt we have n = 0.76. A rough approximation to the dependence of M_s on the source and source material properties is then

$$M_s \approx \log \left[\mu_s^{3/4} \, \dot{\Psi}_\infty \right], \tag{16}$$

where $\dot{\Psi}_\infty$ is the (nearly constant) low frequency value of $\dot{\Psi}$. This equation should be approximately be valid for all NTS

source regions since the change from tuff to granite in the top two kilometers of the path model (Table 1) for this example is about the most severe change we expect to encounter.

4.4 THE DEPENDENCE OF M_s ON EPICENTRAL DISTANCE

The M_s values presented in the previous section were for a particular epicentral distance (3000 km). In that section we were interested in the change in M_s with yield, burial depth and source material. In subsequent sections the absolute value of M_s will be of interest and we should determine how well this quantity is defined by our theoretical analysis.

In Figure 12 we show seismograms at several ranges for the case in which the yield is 60 kt and the depth is 0.42 km in granite. For each of these records the amplitude of the cycle with period closest to 20 seconds was measured and M_s was computed according to two formulas. One is that used by Eisenhauer [1976] and given in (11). The other is the formula suggested by Marshall and Basham [1972] which is

$$M_s = \log \frac{A}{2} + B'(\Delta) + P(T) \ , \qquad (17)$$

where $B'(\Delta)$ and $P(T)$ are tabulated in the Marshall and Basham paper (the $P(T)$ appropriate for continental North America was selected).

In Table 2 the M_s data for the seismograms of Figure 12 are summarized. The Eisenhauer formula gives M_s values that are 0.16 to 0.21 units larger than those from the other formula. The scatter is slightly greater for the values from the Marshall and Basham formula. The 3000 km theoretical record gives a theoretical M_s that is close to the "average" value, though it

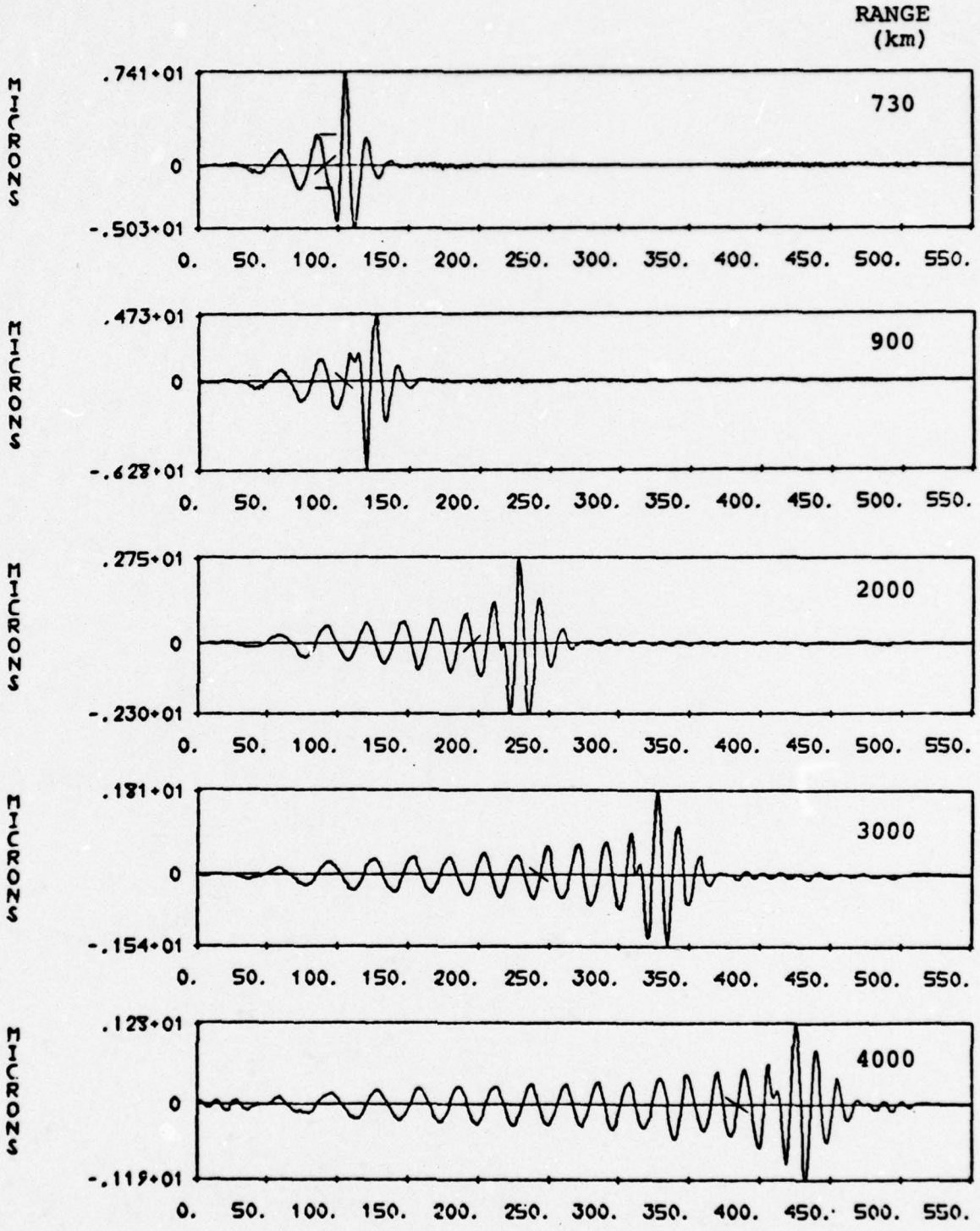

Figure 12. Theoretical seismograms are shown for five epicentral distances for the granite source with yield 60 kt and depth 0.23 km. The cycle at which the M_S measurement is made is indicated with a bar.

TABLE 2

M_s VALUES FROM THE SEISMOGRAMS OF FIGURE 11

Range (km)	Amplitude (km)	Period	M_s (Eisenhauer)*	P(T)	M_s (Marshall & Basham)
730	4780	18.5	4.32	-0.12	4.14
900	4419	18.9	4.37	-0.09	4.21
2000	2123	19.4	4.40	-0.05	4.19
3000	1219	19.7	4.34	-0.03	4.13
4000	1085	19.9	4.41	-0.01	4.24
Average M_S			4.37		4.18

*We have corrected for the instrument response at the actual period rather than at 20 seconds, which may or may not be consistent with common practice. The difference this may cause is small, a few hundredths of a unit at most.

is perhaps a bit low. It seems reasonable to use the M_s from records at 3000 km as our theoretical M_s estimate.

4.5 THE DEPENDENCE OF M_s ON PROPERTIES OF THE TRAVEL PATH

For computing theoretical surface wave seismograms we are using two crustal models, one for the crust in the vicinity of the source and one for the "average" crust between the source and receiver. Even if the source were azimuthally symmetric, the radiated surface waves may be asymmetric due to azimuthal differences in the travel path. To get some idea of how strong this effect might be, we computed a series of theoretical seismograms with the source region crust being fixed while a number of different continental crustal models were used for the rest of the path.

The velocity-depth profiles for the various crustal models are shown in Figure 13. The source region model is one proposed by McEvilly [1964] with the low velocity surface sedimentary layer replaced by PILEDRIVER granite. This model is much like the Alexander [1963] model 35-CM2 with a granite cap discussed in Section 3.2. The other models are:

B - A North American crustal model from McEvilly [1964]

C - Model 35-CM2 from Alexander [1963]

D - CIT 109 due to Archambeau, et al., [1969] and based primarily on body waves from NTS explosions

E - A model with an NTS granite crust over a mantle derived by Helmberger (private communication from Harkrider, 1977)

F - A Gutenburg continental model taken from a paper by Harkrider, et al., [1963]

G - An average earth model constructed by D. Anderson that is essentially a monopole fit to the free oscillation data.

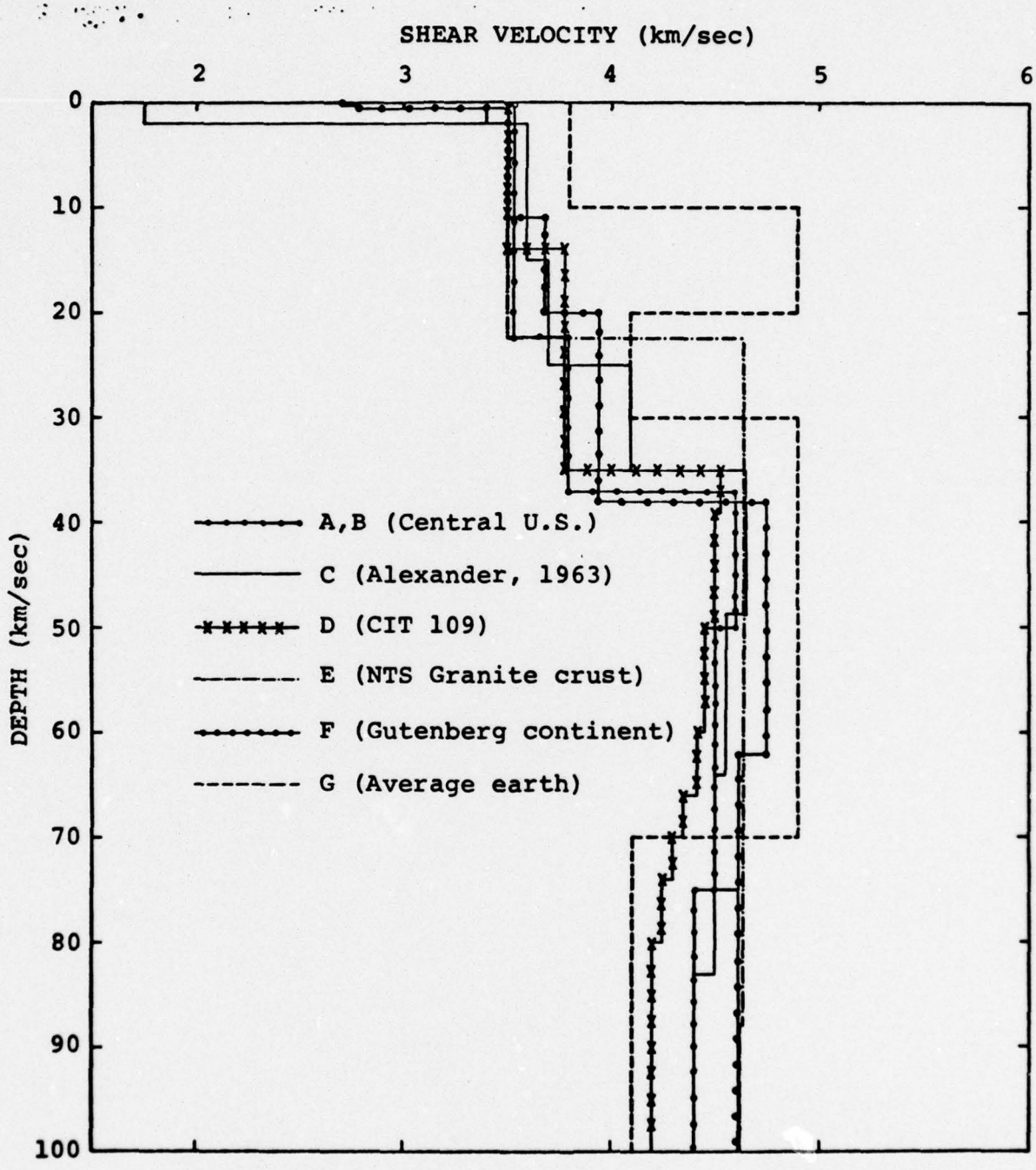

Figure 13. The shear wave velocity is plotted versus depth for seven crustal models.

The phase and group velocity curves for these structures are shown in Figure 14.

As is apparent from the formula (10), the other quantity of importance for computing surface waves is the transmission coefficient, $T(\omega)$. Since all these structures are pretty much the same, this coefficient is close to unity. In fact, for models B, D, E, F and G the value at 20 seconds ranges from 0.97 to 1.03. For model C, the average earth model, the structural contrast is greater than for the continental models and $T(\omega)$ at 20 seconds is 0.87.

Aside from the $T(\omega)$, the only influence of the average crust model (when the source region model is fixed) is in the propagation term, the Hankel function in (10). Then when $T(\omega)$ is nearly unity as it is for the cases discussed here, the amplitude spectra are nearly the same near 20 seconds for all the path models. Differences in the 20 second component in the time domain are due to interference effects.

Synthetic seismograms at 3000 km are shown in Figure 15 for the seven path models. The M_s data are summarized in Table 3 in the same format as Table 2. The values scatter by a little less than 0.2 M_s units. This scatter is an indication of how difficult it is to get a good, consistent estimate of the amplitude of the 20 second component of the dispersed wave.

4.6 THE EFFECT OF SUPPRESSION OF THE UPWARD TRAVELING WAVES GENERATED BY THE SOURCE

In Section 3.2 we outlined several potential problems that arise when the explosion is represented by a spherically symmetric source of elastic waves embedded in one layer of a layered earth model. We noted the fact that for most events the nonlinear region intersects the free surface. Also, we know the source region is inhomogeneous; the coupling

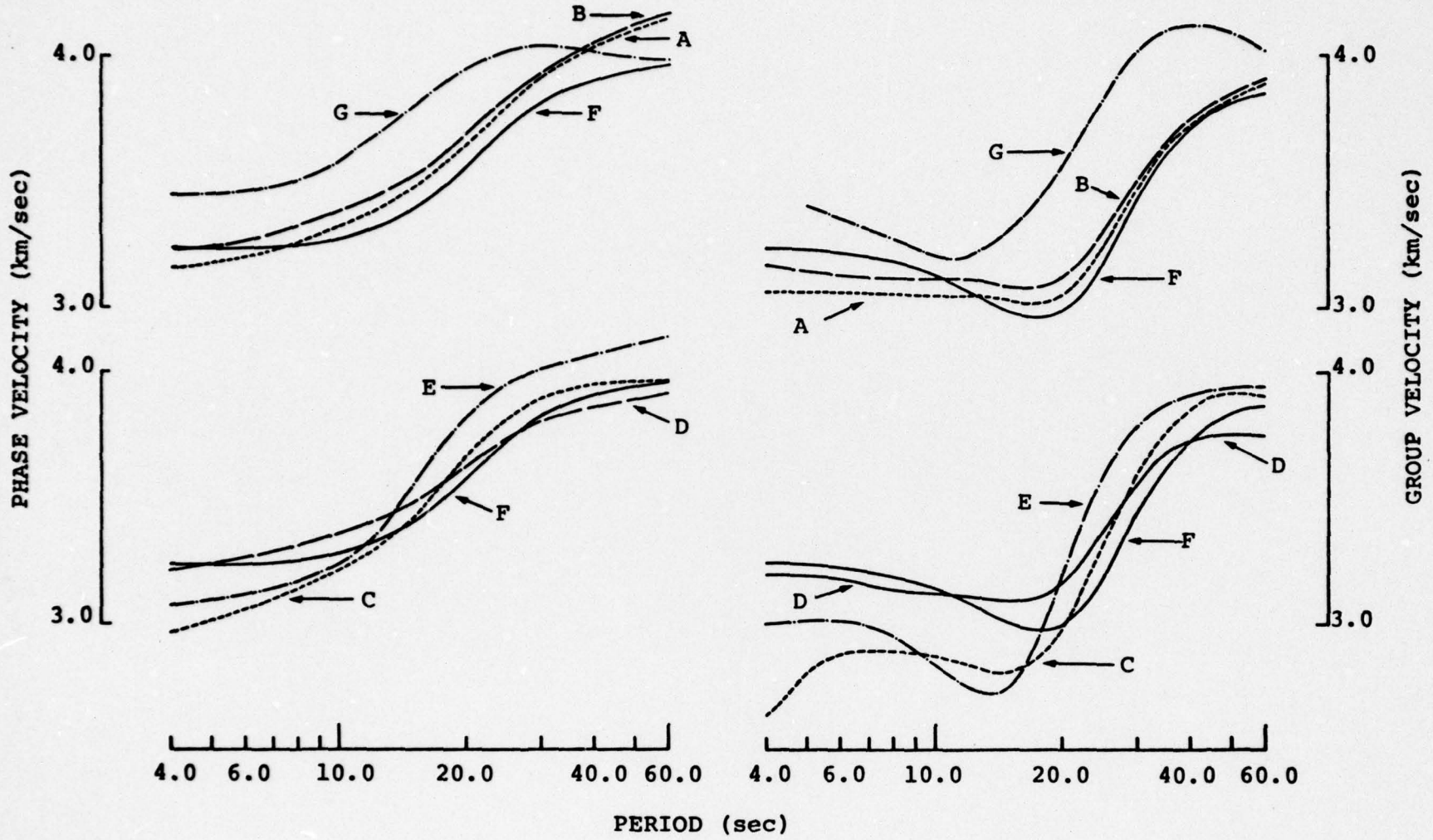

Figure 14. The Rayleigh wave phase (left) and group (right) velocities are plotted for the structure of Figure 13.

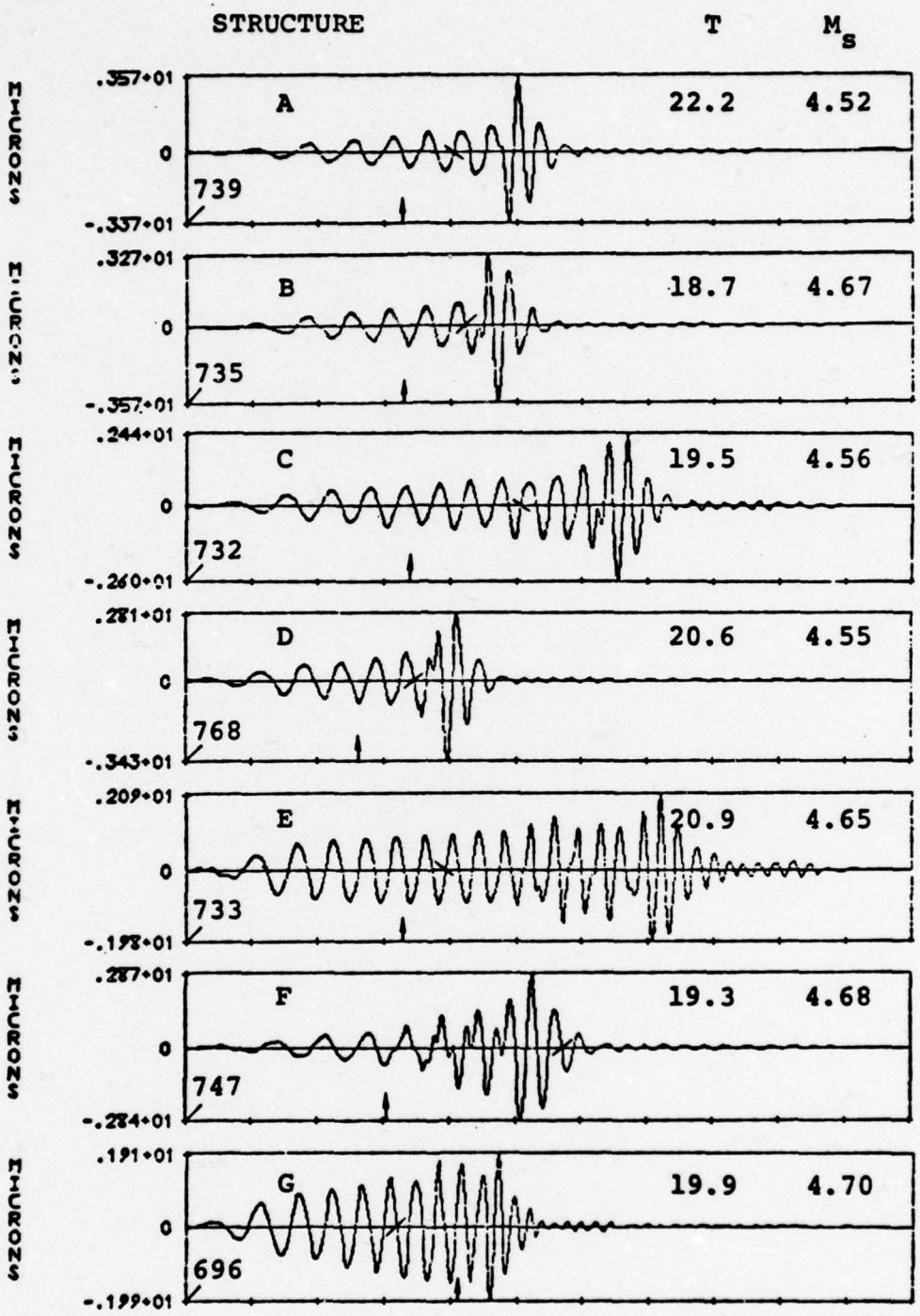

Figure 15. Synthetic seismograms are shown for a 100 kt explosion at a depth of 0.7 km, using a mixed path model. The source region model is A and seven average path models are used. The time corresponding to zero on the scale is indicated on each record as well as the M_s (using (11)) and M_s period. A small arrow on the time axis marks 900 seconds after detonation time. The cycle at which the M_s measurement is made is marked with a bar. At the left is amplitude in microns at 25 seconds.

TABLE 3

M_s VALUES FROM THE SEISMOGRAMS OF FIGURE 15

Path Structure	Amplitude (mμ)	Period	M_s (Eisenhauer)	P(T)	M_s (Marshall & Basham)
A	1864	22.2	4.52	0.03	4.38
B	2640	18.7	4.67	-0.11	4.39
C	2053	19.5	4.56	-0.4	4.35
D	2009	20.6	4.55	0.1	4.39
E	2523	20.9	4.65	0.1	4.49
F	2661	19.3	4.68	-0.6	4.45
G	2818	19.9	4.70	-0.1	4.52

properties of materials above and below the source are not the same. The most obvious difference is the fact that the "average" overburden pressure in the inelastic region above the source is lower than in the analogous region below the source. Lower overburden pressures generally lead to larger source functions. Acting in the opposite direction is the effect of the generally higher air-filled porosity above the source. Perhaps more important is the fact that at least some energy is lost from the upgoing wave due to spallation. The upgoing wave would also seem to be more subject to losses due to scattering and inelastic attenuation in the immediate vicinity of the source than the downgoing wave. At present we do not really know how important these various effects are. We need to carry out some theoretical studies involving two-dimensional finite difference calculations to develop a better understanding. Even so, with our relatively simple models we can do some things to better delineate the effects these source asymmetries might have.

Our theoretical formulation for both body and surface waves has been modified to allow total or partial suppression of the source radiation emitted upward or downward from the source (Harkrider and Bache [1977]). This allows us to do several things to better understand the effects being discussed. First, we can hypothesize that the waves traveling upward from the source (takeoff angles above the horizontal) are trapped or scattered or in some way prevented from coupling into the far-field Rayleigh wave. We can then compare the Rayleigh wave amplitudes or M_s from the total source to those from the same source with the upward traveling waves suppressed. A second useful thing to do is to suppose that the equivalent elastic source ($\Psi(\omega)$) is different for the upgoing and downgoing waves. In fact, since the geologic environment is generally different above and below the source,

we can obtain first order estimates of how different these sources might be with relatively inexpensive one-dimensional source calculations. Even without such source calculations, we can delineate the range of possible effects since we believe the source function is nearly constant over the frequency band of interest for surface waves. Thus, one-dimensional sources can be represented by a single number, Ψ_∞. A simple way to investigate the question is then to suppose that the size of the Ψ_∞ appropriate for the upgoing waves is different than that for the downgoing waves.

Let us return to the calculations of Section 3.3 for which theoretical seismograms are shown in Figures 8 and 9. The question is, what is the effect of totally or partially suppressing the upgoing waves excited by the source? This effect is delineated for one case by the seismograms shown in Figure 16. The example studied is the granite source, 60 kt yield, 0.42 km depth case from Figure 8. We show the seismograms for the upgoing and downgoing waves separately and for their total, which is the same as the corresponding record in Figure 8. Seismograms computed with the source (Ψ_∞) for the upgoing waves being 0.25, 0.50 and 0.75 times the size of the source for the downgoing waves are also shown. For this case the surface waves for the up and down-going waves are almost exactly in phase. The addition of various fractions of the upgoing wave portion of the source then has rather simple and predictable effects.

In Figure 17 we study the contribution of the up and downgoing portions of the source for an event just like that in Figure 16 except that the source is in tuff. For this case the seismogram for the upgoing portion of the source is nearly the negative of that for the downgoing portion with a slight shift to later time. Then in contrast to the results for the source in granite, addition of the two portions of the source leads to destructive interference and a reduction in M_s.

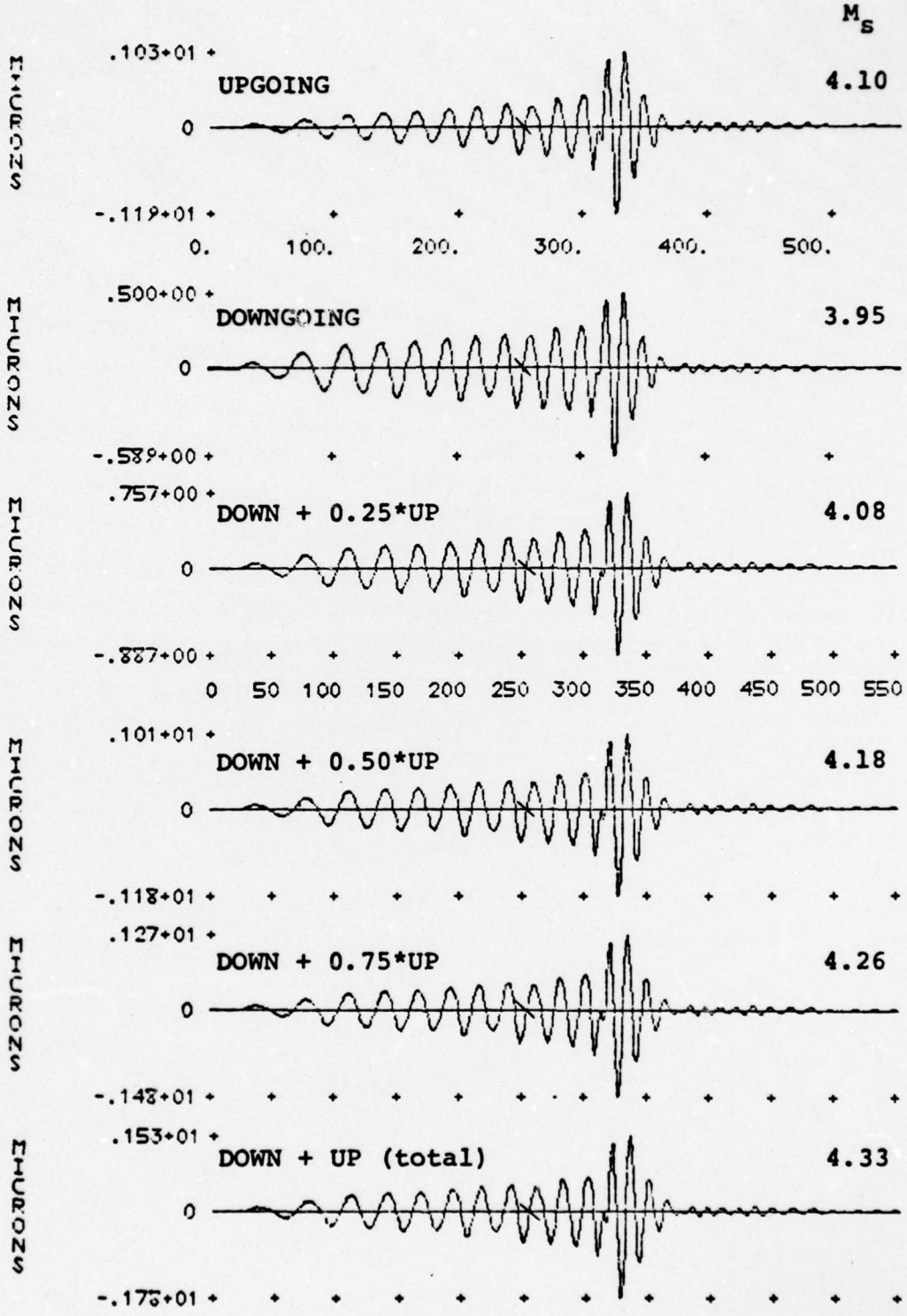

Figure 16. Seismograms are shown for the 60 kt granite source at 0.42 km depth from Figure 8. The upgoing wave and downgoing wave contributions to the source are shown separately. The seismograms for the downgoing wave portion added to the indicated fraction of the upgoing portion are also shown. Note that the polarity is reversed from earlier seismograms (positive vertical is up).

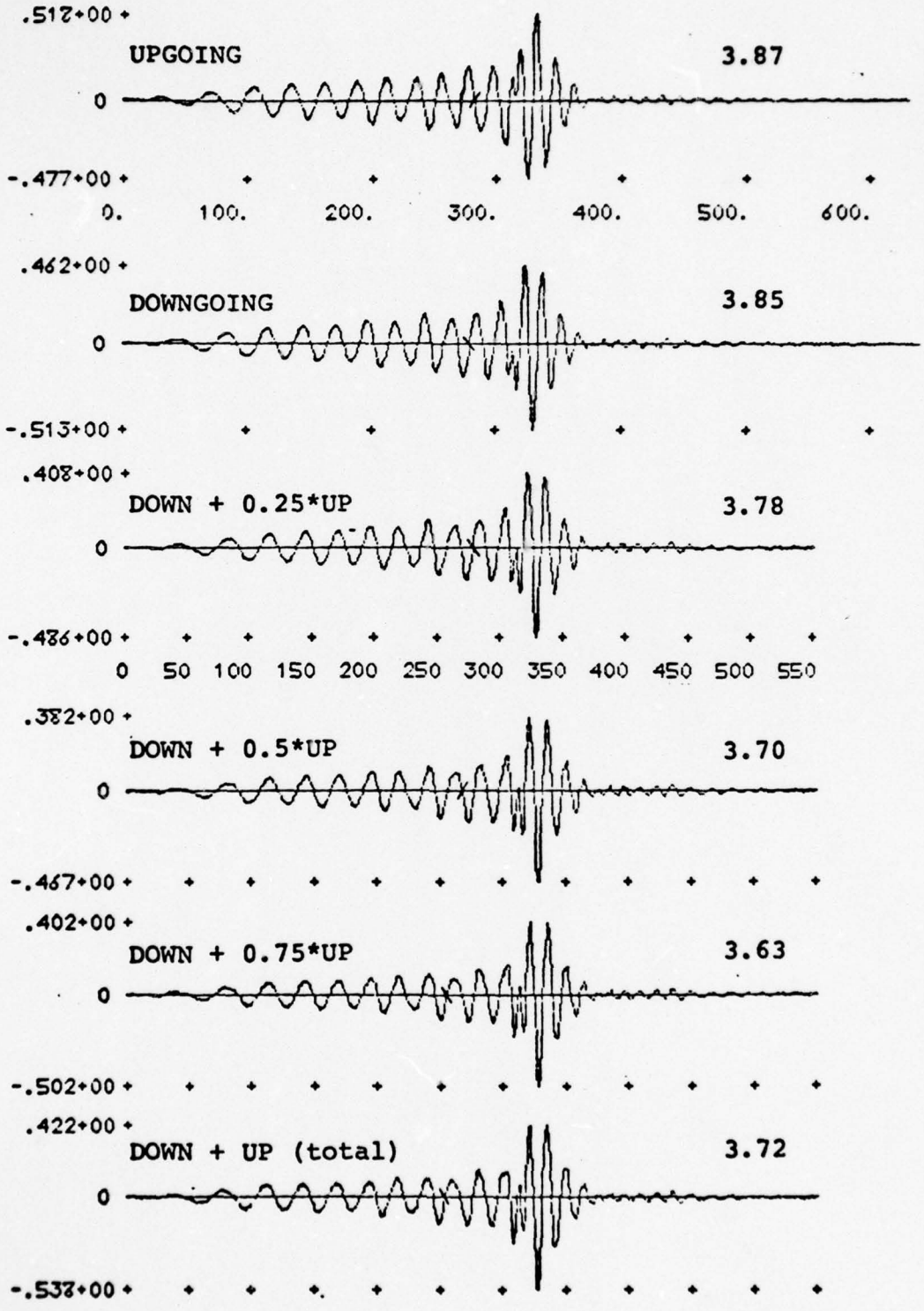

Figure 17. Seismograms are shown that are identical to those in Figure 16 except that the source is in tuff.

While some part of the M_s variation in Figure 17 is due to shifts in the phase at which the amplitude is measured, comparison of the 20 second spectral amplitudes for these seismograms gives much the same result.

What is the effect of suppressing the upward traveling waves on the M_s-yield curves? In Figures 18 and 19 we show seismograms for the same events as in Figures 8 and 9 except that the upward traveling waves are entirely suppressed. As was the case in Figures 8 and 9, we note that changes in burial depth over this range have essentially no effect on the waveform. The M_s values are plotted versus yield in Figure 20 together with least square fits to these data and the analogous data from Figure 10. The only really significant effect of suppressing the upgoing waves is that noted in connection with Figures 16 and 17; the M_s is reduced for the granite source and is enhanced for the tuff source.

Let us now summarize what we have learned from the examples of this section. It seems quite plausible to suppose that the upgoing wave is suppressed to some degree compared to the downgoing wave for many explosions. For a source in a low strength material overlying a hard basement, we find that the surface wave excited by the upgoing waves is about 225° out of phase with that associated with the downgoing wave. Suppression of the upgoing wave then acts to increase M_s compared to that for the total source. On the other hand, when the source is in hard rock, the two portions of the surface wave are in phase and suppression of the upgoing wave reduces the M_s. Recall that we found (Section 4.3, Equation (16)) for the total source that $M_s \approx \log [\mu_s^{3/4} \Psi_\infty]$. When the upgoing wave is totally or partially suppressed, the depenence on μ_s is much weaker. In fact, for total suppression of the upgoing wave we find that

$$M_s \approx \log [\mu_s^{1/8} \Psi_\infty] \ . \qquad (18)$$

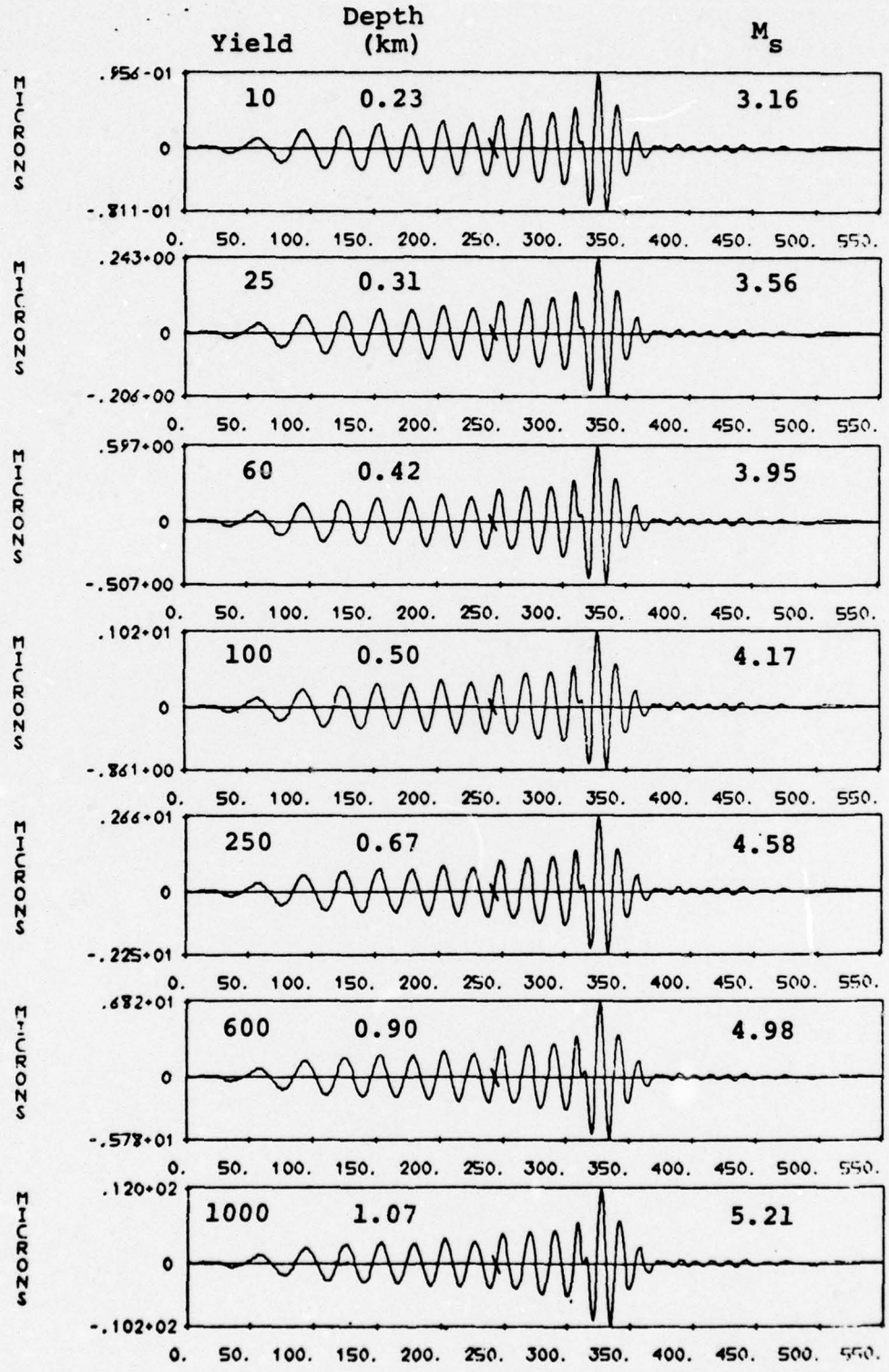

Figure 18. Theoretical seismograms are shown that are identical to those of Figure 8 (the source is in granite) except that the upgoing waves are suppressed. Positive vertical is down.

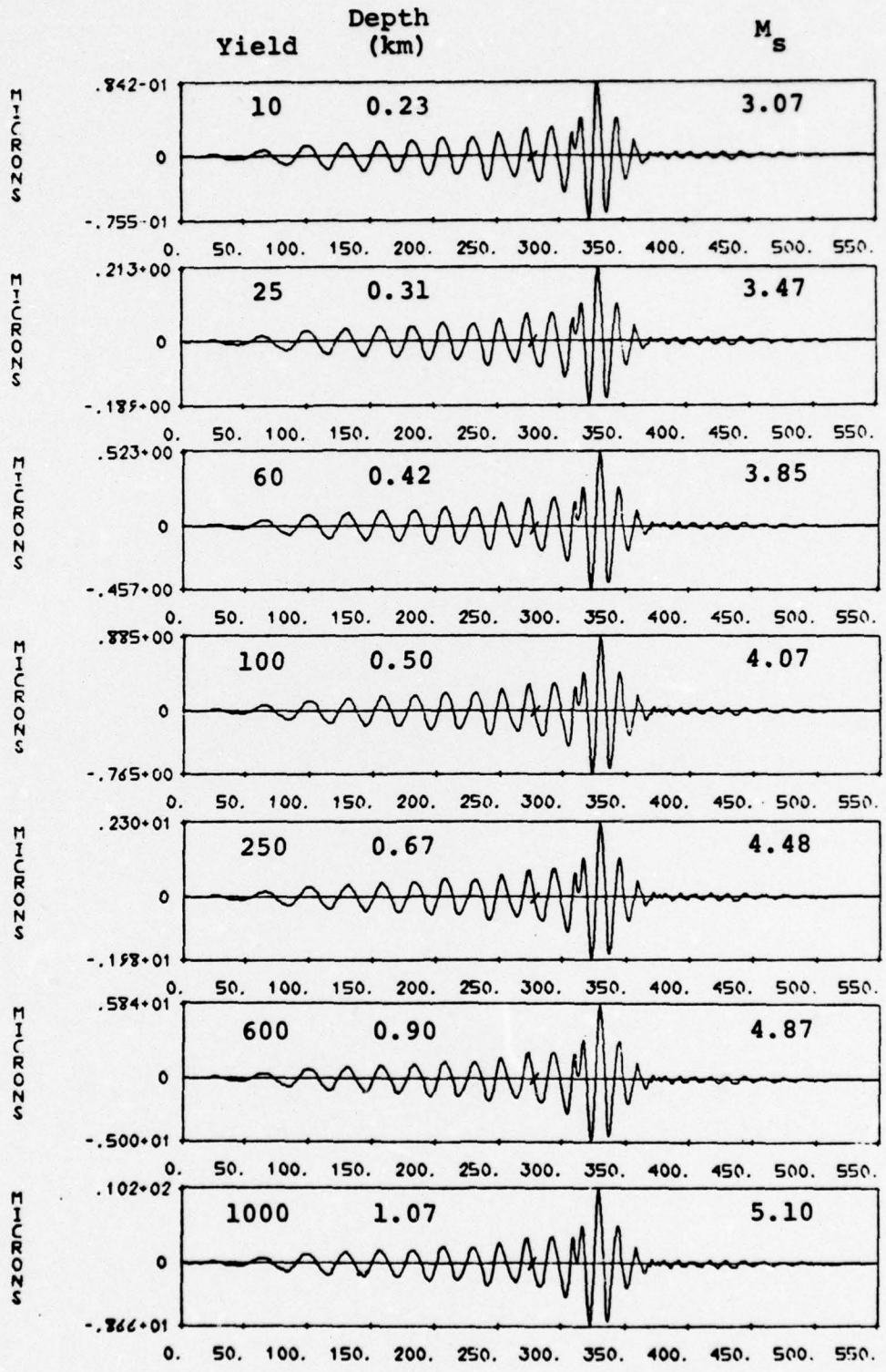

Figure 19. Theoretical seismograms are shown that are identical to those of Figure 9 (the source is in tuff) except that the upgoing waves are suppressed. Positive vertical is down.

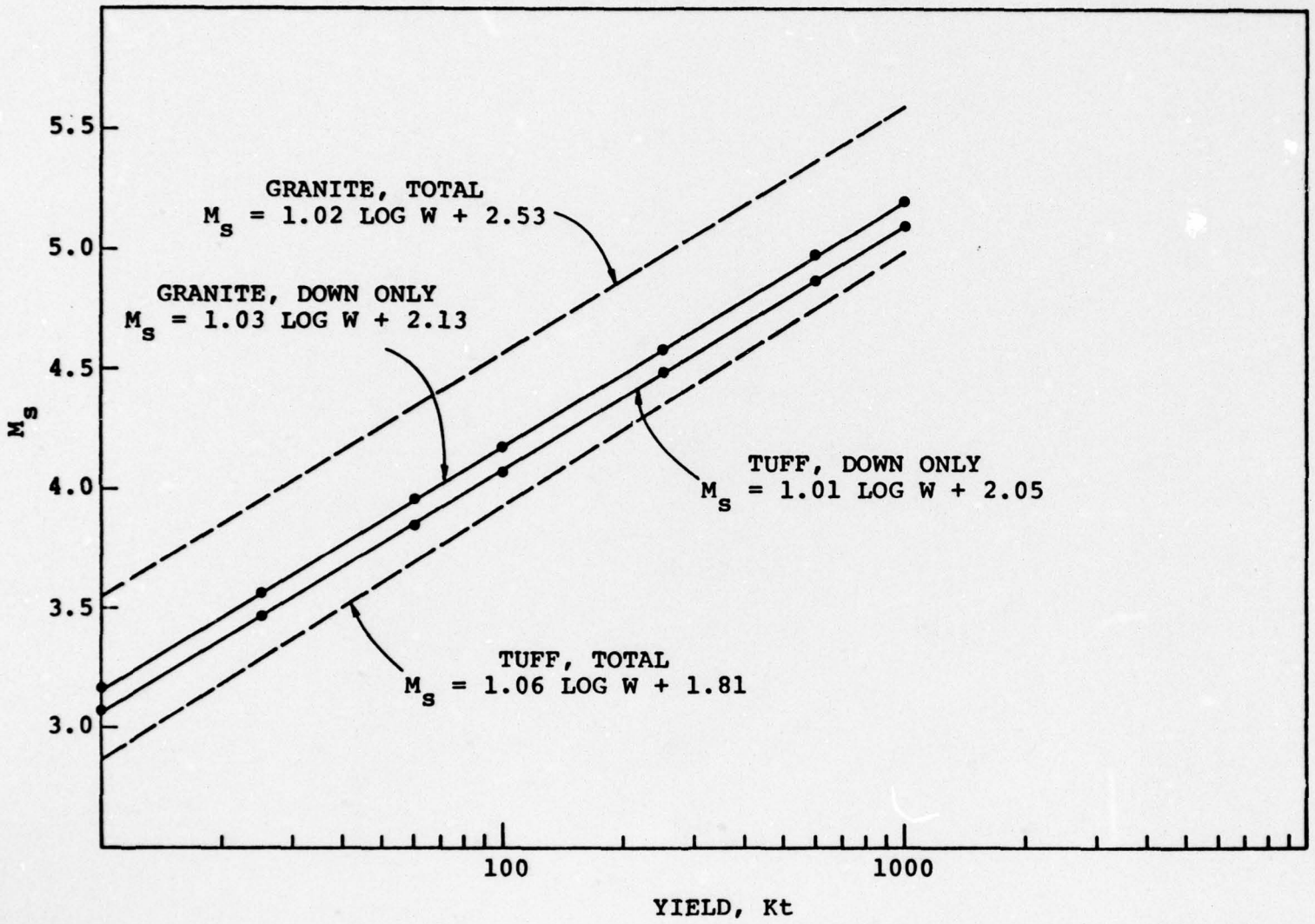

Figure 20. The M_s values from Figures 18 and 19 are plotted versus yield. The results of a linear least squares regression assuming all error is in M_s are shown for each data set and for the analogous data from Figure 10.

That is, in this case the M_s is nearly independent of the properties of the source medium other than indirectly via $\Psi(\omega)$.

V. SIGNAL DECONVOLUTION

5.1 INTRODUCTION

Teleseismic signals are controlled by characteristics of the source and the travel path. Since most underground nuclear tests are conducted in a small number of known test sites, there are fairly large populations of events for which the path effects should be about the same. Even comparing events at different test sites, local station effects might be expected to be stationary. In short, it should be possible to isolate some components of the transfer function relating the explosion source to the teleseismic waveform and, thereby, improve our ability to isolate the source effects.

To be more explicit, let us express the teleseismic short period signal in the following form:

$$u = T_I \cdot T_{RC} \cdot T_M \cdot T_{SC} \cdot T_{ES} \cdot W \,, \qquad (19)$$

where W is the yield of the explosion and the T represent the transfer functions that relate the explosion to the recorded waveform. The T_{ES} represents the conversion of the energy of the explosion into elastic waves in the earth and depends on the local materal properties. The most one could hope for with seismic methods is to estimate the equivalent elastic source, or $T_{ES} \cdot W$. The T_{SC}, T_M and T_{RC} break the travel path into three segments, the crust at the source, the upper mantle and the crust at the receiver. The T_I is the transfer function of the seismometer and is easy to remove.

How can we "deconvolve" recorded seismograms to isolate and quantify these transfer functions? There are several schemes that come to mind:

1. Consider a series of teleseismic recordings of the same event. The common part should

be $T_I \cdot T_{SC} \cdot T_{ES} \cdot W$. If this can be extracted and deconvolved with the seismograms, the residual should be $T_M \cdot T_{RC}$. We will know how well this works by how constant $T_M \cdot T_{RC}$ is from event-to-event.

2. Consider a series of similar events recorded at a particular station. The common part should be $T_I \cdot T_{RC} \cdot T_M$ and the residual is then $T_{SC} \cdot T_{ES} \cdot W$. The $T_I \cdot T_{RC} \cdot T_M$ should be nearly constant from event-to-event.

3. Having done previous study, we can further analyze the $T_I \cdot T_{RC} \cdot T_M$ to determine T_{RC}. The T_I is known and the T_M should be nearly independent of frequency for most stations beyond 35° or 40°. We then can estimate T_{RC} for the particular station under study. We hope this T_{RC} would be fairly constant from event-to-event, though it may exhibit some range (incidence angle) and azimuthal dependence.

We have outlined what we would like to be able to achieve by deconvolving teleseismic short period recordings of underground explosions. In the remainder of this section we outline the method we plan to use which is closely related to the homomorphic deconvolution method described by Clayton and Wiggins [1976].

Many schemes have been suggested for inverting seismic data to isolate the signal that is common to all the observations. Problems of this nature belong to the type designated through various names: deconvolution, inverse filtering, decomposition, etc. All these operations, being

of the inverse type, are characterized by their potential instabilities. In this respect, they are all similar to the simple inverse arithmetical operation, i.e., the division, the inverse of the multiplication operation. If the divisor gets to be very small, the inverse grows to very large size and greatly magnifies the quantity on which it operates. If this quantity is not known with sufficient accuracy or is contaminated with noise, the result of the operation becomes meaningless.

Deconvolution or decomposition of a given signal is entirely controlled by the assumptions that the user of the technique is willing to make. If these assumptions are valid and the data fits the model they imply, deconvolution can be a powerful tool indeed; if, on the contrary, they are irrelevant, the results may be very discouraging or even disastrous.

Estimating a source signature is equivalent to performing the decomposition of an observation, sometimes called an output, into its two basic components: a waveshape, also called the input, and a response or transfer function.

Response or transfer function analysis originated primarily in the electrical engineering field and, in that field, it has branched out in several separate expertises such as network analysis, filter design, time series analysis, information and communication theory, control theory, etc. More recently, it has been extensively applied and adapted to the seismic exploration area, particularly with the introduction of optimal filtering and deconvolution techniques in the early fifties.

In exploration reflection seismology, most deconvolution techniques rely on the assumption that there are enough events of constant shape in a single trace over the time interval of interest that the theory of stationary time series applies. This is equivalent to saying that the transfer

function or response is white while the wave shape has minimum phase characteristics. With these two assumptions, the decomposition is unique and the answer can be obtained from a single autocorrelation analysis. The autocorrelation of the signal determines the power spectrum from which the minimum phase waveshape can be derived and its inverse used to perform the deconvolution of the trace. Unfortunately, these assumptions appear unrealistic in the case of teleseismic events. We must then resort to a different approach.

Another approach to deconvolution was developed in the late sixties by generalizing the notion of superposition through the introduction of a nonlinear homomorphic transformation, the logarithmic operation. Just remember how, through the logarithmic operation, the arithmetical operation of multiplication is reduced to an addition, a very substantial simplification. Similarly, when considering the convolution operation, note that in the frequency domain it reduces to a complex multiplication. Therefore, if one makes a logarithmic transformation in the spectral domain, the multiplication reduces to a mere addition. This sounds too good to be true and, in fact, we are going to show that it is not quite that simple, but it is worth pursuing.

The spectrum of a signal is generally a complex quantity and the logarithm of a complex quantity is not single valued, since if $z = \rho e^{i\theta} = \rho e^{i(\theta+2K\pi)}$ $\ell n\ z = \ell n\ \rho + i(\theta+2K\pi)$ where K is any positive or negative integer. Thus, we have an inherent ambiguity in using the spectral route. However, in a way similar to the minimum phase assumption in the ordinary deconvolution, we may be able to remove the 2π ambiguity by making again further assumptions.

This deconvolution technique, called homomorphic deconvolution, has been used by several teleseismic analysts who think that it is better adapted to the processing of

teleseismic recordings than the deconvolution techniques employed in seismic exploration. They claim it is particularly well adapted to echo removal or dereverberation. In order to see why, we must first describe more precisely what homomorphic deconvolution is.

Assume a given signal, s(t), it is known to be the result of the convolution of two other signals, a waveshape w(t) and a response r(t). Then

$$s(t) = w(t)*r(t) = \int_{-\infty}^{t} w(t)r(\tau-t)\, d\tau = \int_{-\infty}^{t} r(t)w(\tau-t)\, d\tau \ . \qquad (20)$$

In the frequency domain this translates into

$$S(\omega) = W(\omega) \cdot R(\omega) = |S(\omega)|\, e^{i\theta(\omega)} = |W(\omega)| \cdot |R(\omega)|\, e^{i(\Phi(\omega)+ (\theta))}, \qquad (21)$$

where capital letters are used to represent Fourier transforms of the corresponding signal which is denoted by a small letter. Taking the logarithm, we have

$$\ell n\, S(\omega) = \ell n\, |S(\omega)| + i\theta(\omega) = \ell n\, |W(\omega)| + \ell n|R(\omega)| + i\,[\phi(\omega) + \Psi(\omega) + 2K\pi] \ . \qquad (22)$$

A new quantity is then introduced by taking the inverse Fourier transform of the $\ell n\, S(\omega)$. This produces a signal which, while it is real, has been named the complex cepstrum to differentiate it from the real cepstrum (e.g., reference) which uses the same transformation on the power spectrum, a real quantity. The real cepstrum is in the time domain, but to retain the distinction between it and the original input signal, this new domain is called the quefrency domain.

Our technique for a signal deconvolution takes the following form. Given a number of signals having a good degree of similarity, we first take their Fourier transform to derive for each signal its amplitude spectrum and its phase in the usual $(-\pi,\pi)$ interval. The phase is then unwrapped in a very simple way. If the phase moves from the second to the third quadrant, 2π is subtracted. If it goes from the third quadrant to the second, 2π is added. In this way, we obtain a reasonably smooth phase if the sampling rate produces a high enough Nyquist frequency. Actually, the criterion used is whether $\Delta\phi = \phi(i+1) - \phi(i)$ is greater than $3\pi/2$ or smaller than $-3\pi/2$. When the phase moves from the second quadrant to the third, $-\pi \leq \phi(I) \leq -\pi/2$ and $\pi/2 \leq \phi(I+1) \leq \pi$, so that $\pi \leq \Delta\phi \leq 2\pi$. Similarly, when the phase moves from the third quadrant to the second, $\pi/2 \leq \phi(I) \leq \pi$ and $-\pi \leq \phi(I+1) \leq -\pi/2$, so that $-2\pi \leq \Delta\phi \leq -\pi$. The selection of $3\pi/2$ equally distributes the probabilities. Another approach would be to add and subtract 2π to the $\Delta\phi$ value and select the one of the three choices which has the smallest absolute amplitude. After the phase has been unwrapped, the logarithmic transformation is performed to produce a complex quantity ($\ln S(\omega)$) for each signal.

The next step is to arithmetically average the amplitude and phase of the logarithm of the transform for each signal. That is, if we had N signals with transforms

$$S_i(\omega) = |W(\omega)||R_i(\omega)|\, e^{i\phi(\omega)}\, e^{i\psi_i(\omega)}, \quad i = 1, N, \tag{23}$$

then

$$\ln S_i(\omega) = \ln|W(\omega)| + \ln|R_i(\omega)| + i\,[\phi(\omega) + \psi_i(\omega) + 2K\pi + 2J_i\pi], \tag{24}$$

where K and J_i are integers. The averaging is then done according to

$$A(\omega) = \frac{\sum_{j=1}^{N} [\ell n|W(\omega)| + \ell n|R_i(\omega)|]}{N} ,$$

$$B(\omega) = \frac{\sum_{i=1}^{N} [\phi(\omega) + \psi_i(\omega) + 2K\pi + 2J_i\pi]}{N} , \tag{25}$$

with the average logarithmic spectrum being

$$X(\omega) = A(\omega) + iB(\omega) \quad . \tag{26}$$

The spectrum of the average source shape is then

$$Y(\omega) = e^{A(\omega)} \; e^{iB(\omega)} \quad . \tag{27}$$

The agreement between $Y(\omega)$ and the common wave shape, $W(\omega)$, then depends on how symmetrically the $R_i(\omega) \cdot W(\omega)$ are distributed about the $W(\omega)$.

For a final estimate of the average signal, it is often advantageous to truncate or smooth the spectrum $Y(\omega)$. We are currently applying a cosine taper to the high frequency portion of $Y(\omega)$. Our results indicate that most of the important information is contained in the low frequency portion of the spectrum and rather severe low pass filters can be applied without seriously affecting the solution.

Estimating a signal shape is tricky business requiring adequate understanding of the various factors controlling the presence of the signal shape in the individual data inputs.

A common problem is that of time relationship, another is that of noise contamination and still a third one is complexity of the source. An adequate procedure must make optimum use of the information contributed by each input signal. The scheme we have just described appears to do that adequately, probably because the spectral averaging through the logarithmic transformation leads to a geometric average instead of an arithmetic one, thus reducing even more the variations from the average.

In Section 5.1 we set forth the criterion by which the adequacy of this technique is to be judged; that is, by the degree by which the transfer functions remain the same from one set of data to another. To make this judgment, we need to test the technique on a representative sampling of data and such tests are now underway. As an indication of the results, a few simple examples are shown in the following section.

5.2 PRELIMINARY RESULTS

The first sampling of seismograms analyzed consists of four recordings of an intermediate yield explosion at Pahute Mesa, NTS. The event is MAST and the recordings are shown in Figure 21. At the bottom of the figure are two examples of the average wavelet present in these data. First shown is the average of all four seismograms. Then station EBC was dropped and the remaining three traces were averaged. Comparing the two, we get some indication of how much the average time signal can vary by increasing or decreasing the number of traces used in the average. Of course, the more pertinent question is how sensitive the transfer function at individual stations is to this average.

A second example is shown in Figure 22. In this case we have seven recordings of a presumed Soviet explosion. The

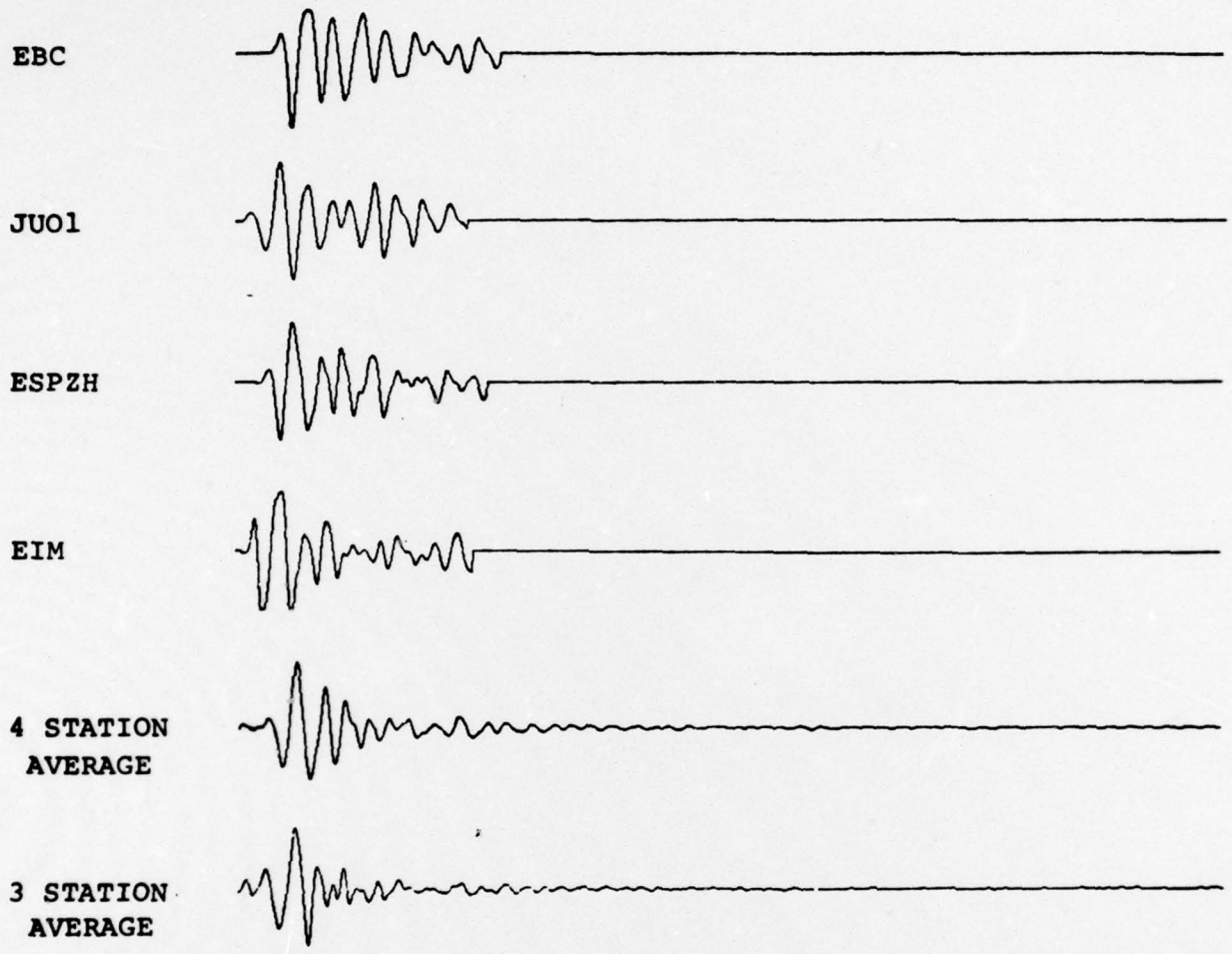

Figure 21. Comparison of average wavelets determined from MAST seismograms at 4 Stations (EBC, JUO1, ESPZH and EIM) and 3 Stations (JUO1, ESPZH and EIM).

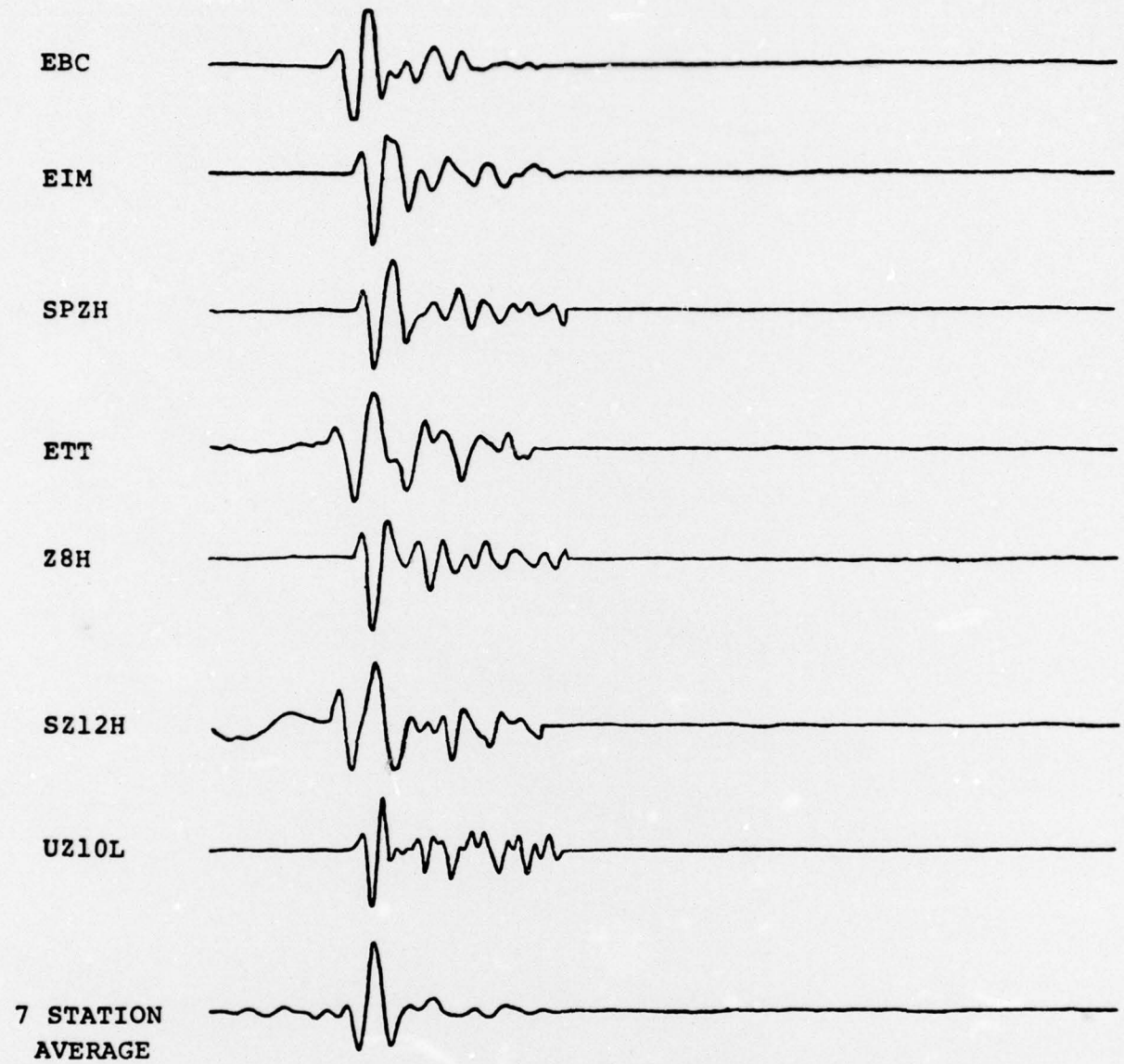

Figure 22. Average wavelet determined from a single event recorded at seven stations.

interesting thing about the average signal is that it is a quite discrete pulse having about the shape we expect for a buried explosion. Once again, we must say that we need to compute more examples and, especially, study the transfer functions, to quantify how good this average pulse is.

In summary, we have developed a signal averaging or decomposition scheme that is rather simple to implement and apply. The crucial operation in applying this technique is the unwrapping of the phase of the spectrum of the individual signals. A few very preliminary examples show that the technique derives an average signal that seems to be reasonable for the data being processed. The next step, which is now underway, is to compute transfer functions from which the validity and utility of the technique can be judged according to the criteria set forth in the introduction to this section (Section 5.1).

REFERENCES

Alewine, R. W., [1974], "Application of Linear Inversion Theory Toward the Estimation of Seismic Source Parameters," Ph.D. Thesis, California Institute of Technology.

Alexander, S. S., [1963], "Crustal Structure in the Western United States from Multi-Mode Surface Wave Dispersion," Ph.D Thesis, California Institute of Technology.

Archambeau, C. B., E. A. Flinn and D. G. Lambert, [1969], "Fine Structure of the Upper Mantle," J. Geophys. Res. 74, pp. 5825-5865.

Archambeau, C. B. and C. Sammis, [1970], "Seismic Radiation from Explosions in Prestressed Media and the Measurement of Tectonic Stress in the Earth," Rev. Geophys., 8, pp. 473-499.

Bache, T. C., J. T. Cherry, N. Rimer, J. M. Savino, T. R. Blake, T. G. Barker and D. G. Lambert, [1975a], "An Explanation of the Relative Amplitude Generated by Explosions in Different Test Areas at the Nevada Test Site," Systems, Science and Software Final Contract Report, DNA 3958F.

Bache, T. C., J. T. Cherry, K. G. Hamilton, J. F. Masso and J. M. Savino [1975b], "Application of Advanced Methods for Identification and Detection of Nuclear Explosions from the Asian Continent," Systems, Science and Software Semi-Annual Technical Report SSS-R-75-2646.

Clayton, R. W. and R. A. Wiggins [1971], "Source Shape Estimation and Deconvolution of Teleseismic Bodywaves," Geophys. J., 47, pp. 151-177.

Eisenhauer, T. D., [1976], "M_s amd m_b Estimates for USSR Underground Explosions," Unpublished Report.

Harkrider, D. G., A. Hales and F. Press, [1963], "On Detecting Soft Layers in the Mantle by Rayleigh Waves," BSSA, 53, pp. 539-548.

Harkrider, D. G., [1964], "Surface Waves in Multilayered Media I. Rayleigh and Love Waves from Buried Sources in a Multilayered Elastic Half-Space," BSSA, 54, pp. 627-679.

Harkrider, D. G., [1970], "Surface Waves in Multilayered Media II. Higher Mode Spectra and Spectral Ratios from Point Sources in Plane-Layered Earth Models," BSSA, 60, pp. 1937-1987.

Harkrider, D. G. and T. C. Bache, [1977], "Surface Waves Generated by the Suppression of Either Upgoing or Downgoing Seismic Source Waves (Abstract for presentation at 1977 Spring Meeting of the AGU, Washington, D.C.)," EOS, 58, p. 435.

Marshall, P. D. and P. W. Basham, [1972], "Discrimination Between Earthquakes and Underground Explosions Employing an Improved M_s Scale," Geophys. J., 28, pp. 431-458.

McEvilly, T. V., [1964], "Central U. S. Crust-Upper Mantle Structure from Love and Rayleigh Wave Velocity Inversion," BSSA, 54, pp. 1997-2016.

McGarr, A., and L. E. Alsop, [1967], "Transmission and Reflection of Rayleigh Waves at Vertical Boundaries," J. Geophys. Res., 72, pp. 2169-2180.

McGarr, A., [1969], "Amplitude Variations of Rayleigh Waves - Propagation Across a Continental Margin," BSSA, 59, pp. 1281-1305.

Springer, D. L., and R. L. Kinnaman, [1971], "Seismic Source Summary for U. S. Underground Nuclear Explosions," BSSA, 61, pp. 1073-1098.

Toksöz, M. N. and H. H. Kehrer, [1972], "Tectonic Strain Release by Underground Nuclear Explosions and Its Effects on Seismic Discrimination," Geophys. J., 31, pp. 141-161.

Tryggvason, E., [1965], Dissipation of Rayleigh Wave Energy," J. Geophys. Res., 70, pp. 1449-1455.